Published in final edited form as:
J Immunol. 2009 June 1; 182(11): 6969–6984. doi:10.4049/jimmunol.0804337.

Myosin IIA associates with NK cell lytic granules to enable their interaction with F-actin and function at the immunological synapse[1]

Keri B. Sanborn[*], **Gregory D. Rak**[†], **Saumya Y. Maru**[‡], **Korey Demers**[¶], **Analisa Difeo**[§], **John A Martignetti**[§], **Michael R. Betts**[¶], **Rémi Favier**[||], **Pinaki P. Banerjee**[‡,‡], and **Jordan S. Orange**[*,†,#]

[*] Immunology Graduate Group, University of Pennsylvania School of Medicine, Philadelphia, PA, USA 19104

[†] Cell Biology and Physiology Graduate Program, University of Pennsylvania School of Medicine, Philadelphia, PA, USA 19104

[‡] Joseph Stokes Jr. Research Institute of the Children's Hospital of Philadelphia, Philadelphia, PA, USA 19104

[§] Department of Genetics and Genomic Sciences, Mount Sinai School of Medicine, New York, NY, USA 10029

[¶] Department of Microbiology, University of Pennsylvania, Philadelphia, PA, USA 19104

[||] Assistance Publique-Hôpitaux de Paris, CRPP, Armand Trousseau Children's Hospital, 75012; Inserm U790, 94100, Villejuif, France

Abstract

NK cell cytotoxicity requires the formation of an actin-rich immunological synapse (IS) with a target cell and the polarization of perforin-containing lytic granules toward the IS. Following the polarization of lytic granules, they traverse through the actin-rich IS to join the NK cell membrane in order for directed secretion of their contents to occur. We examined the role of myosin IIA as a candidate for facilitating this pre-final step in lytic NK cell IS function. Lytic granules in and derived from a human NK cell line, or ex vivo human NK cells, were constitutively associated with myosin IIA. When isolated using density gradients, myosin IIA-associated NK cell lytic granules directly bound to F-actin and the interaction was sensitive to the presence of ATP under conditions of flow. In NK cells from patients with a truncation mutation in myosin IIA, NK cell cytotoxicity, lytic granule penetration into F-actin at the IS, and interaction of isolated granules with F-actin were all decreased. Similarly, inhibition of myosin function also diminished the penetration of lytic granules into F-actin at the IS, as well as the final approach of lytic granules to and their dynamics at the IS. Thus, NK cell lytic granule-associated myosin IIA enables their interaction with actin and final transit through the actin-rich IS to the synaptic membrane, and can be defective in the context of naturally occurring human myosin IIA mutation.

[1]This work was supported by National Institutes of Health grant R01-AI067946 (to J.S.O.). K.B.S. was supported by National Institutes of Health training grant T32-GM07229.

#corresponding author: Jordan S. Orange, Children's Hospital of Philadelphia, Division of Immunology, Abramson Research Center 1014H, 3615 Civic Center Boulevard, Philadelphia, PA 19104, Phone: (267) 426-5622 Fax: (267) 426-5727, orange@mail.med.upenn.edu.

DISCLOSURES

The authors have no financial conflict of interest.

Keywords

Natural Killer Cells; Human; Cytotoxicity

INTRODUCTION

NK cells are lymphocytes of the innate immune system which are important for defense against cancer and viral infection (reviewed in (1)). NK cells directly kill transformed and infected cells, and also provide costimulation and produce cytokines to enhance immunity. Following NK cell conjugation with a target cell, an IS forms at the contact site. The IS represents an arrangement of molecules that changes over time to enable NK cell functions (2,3). During NK cell cytotoxicity, the IS matures to consist of a peripheral ring of F-actin and adhesion molecules surrounding a secretory domain containing lytic granules (4). Upon initial adhesion to target cells, NK cell activation causes polarization of the NK cell secretory machinery toward the target cell. Lytic granules traffic to the IS via microtubules, and exocytosis of their contents, including granzymes and perforin (5), at the plasma membrane is required for cytotoxicity (6–10). While discrete steps in cytotoxicity have been identified following the movement of lytic granules to the IS with the MTOC, these primarily involve docking and fusion with the cell membrane (11–14). The F-actin cortex at the IS is dense, however, and although the lytic granules may come very close to the membrane via microtubules, the actin accumulated at the IS and bordering a secretory domain may nonetheless present an obstacle to lytic granules reaching the membrane. Therefore, transit through the F-actin-rich cell cortex may present an additional requirement for granule release prior to membrane fusion.

Myosin superfamily members have been defined as important facilitators of immunological function (15–17). Myosins are ATP-dependent motors which generate force and movement along actin filaments and can facilitate cell motility and migration (15,18–20). Nonmuscle myosin IIA, however, may have an additional role in NK cells, as it is present in a heterogeneous protein complex formed in NK cells upon their conjugation with susceptible target cells (21). Myosin IIA is a hexameric protein consisting of two heavy chains, two regulatory light chains, and two essential light chains (reviewed in (22)). The N-terminal portion of the protein binds to actin and is important for ATP-dependent motor function, while the C-terminal portion is involved in filament formation and cargo binding (23–27). Recently, a requirement for myosin IIA in NK cell degranulation was defined (16). Interference with myosin IIA function using the specific myosin II inhibitor blebbistatin (28) or the myosin light chain kinase inhibitor ML-9 (29), or myosin IIA small inhibitory RNA, decreased NK cell cytotoxic activity and exocytosis of lytic granule contents, but did not alter effector-target conjugation or NK cell IS formation (16). While myosin IIA has been implicated in the overall process of NK cell cytotoxicity (16), it is unclear how it enables lytic granule exocytosis.

Mutations in the heavy chain of myosin IIA, MYH9, cause several human disorders, including May-Hegglin anomaly (30–33), characterized by macrothrombocytopenia and leukocyte inclusions. Additional variable somatic abnormalities can occur depending upon the specific MYH9 mutation, however, previous studies of patients with these disorders have not pursued or identified immunological deficiencies. Here, we define a deficiency of NK cell cytotoxicity in four patients with May-Hegglin anomaly resulting from a C-terminal truncation of MYH9 at position 1933 and have defined a potential mechanism by which myosin IIA enables NK cell lytic granule exocytosis. We demonstrate that myosin IIA constitutively interacts with NK cell lytic granules and is required for the functional interaction of lytic granules with F-actin as well as their final approach to the synaptic membrane.

MATERIALS AND METHODS

NK cell preparation

PBMCs were prepared from whole blood obtained from patients or healthy volunteer donors using centrifugation through Ficoll-Paque Plus lymphocyte isolation medium (Amersham Biosciences). Ex vivo NK cells (eNK) were prepared from PBMCs either by negative selection as described (6), or by FACS for $CD56^+CD3^-$ lymphocytes in the cell sorting facility of Children's Hospital of Philadelphia using a BD FACSVantage SE/DiVa cell sorter (BD Biosciences), and were used in experiments immediately after preparation. To expand eNK cells for granule preparation, isolated $CD56^+CD3^-$ NK cells were co-cultured with irradiated allogeneic PBMCs and RPMI 8866 cells in RPMI 1640 media (Gibco) containing 5% human serum (Atlanta Biologicals), 500 U/mL human recombinant IL-2 (NIH AIDS Research and Reference Reagent Program), 5×10^{-5} M 2-mercaptoethanol (Gibco), and 2 μg/mL phytohemagluttinin (PHA, Sigma Aldrich). Following establishment of the culture, additional irradiated allogeneic PBMCs and RPMI 8866 cells were added along with 2 μg/mL PHA every 21–30 days and expanded NK cells were monitored over time to maintain near 90% NK cell purity. Myosin IIA 1933x heterozygous mutant NK cells and/or PBMC were derived from four patients with May-Hegglin Anomaly, possessing a C5797T alteration in exon 40 of the MYH9 gene. Mutation analyses were performed at Duke University, Mount Sinai School of Medicine, the Children's Hospital of Philadelphia according to published methods (32). All human samples were obtained with informed donor consent and were used with the approval of the institutional internal review board for the protection of human subjects at the Children's Hospital of Philadelphia.

Cell lines and cellular evaluation

The immortalized NK cell lines YTS and YTS cells stably expressing GFP (YTS-GFP) or a myosin IIA-GFP fusion protein (YTS-MyoIIA-GFP, described below) were used as model NK cell systems and are described elsewhere (6). 721.221 B-lymphoblastoid cells, K562 erythroleukemia cells, and K562 cells stably expressing CD86 (KT86, previously used and described (6)) were used as target cells. To generate YTS-MyoIIA-GFP cells, 3×10^6 YTS cells were nucleofected using an Amaxa Nucleofector (Amaxa, Inc.) with 2 μg of linearized GFP-human nonmuscle myosin IIA heavy chain plasmid containing a neomycin resistance gene (Addgene) in Amaxa solution R (Amaxa Inc.), using nucleofection program O-017. Transfected cells were selected in G418 sulfate (Cellgro) and repeatedly sorted by FACS to obtain a pure population of GFP-expressing cells. YTS and eNK cell granzyme B and perforin content was evaluated by intracellular flow cytometry using fluorophore-conjugated mAbs (BD Biosciences).

Inhibitors

NK cells were pre-incubated with 40 μM ML-9 (Sigma-Aldrich) in 0.5% ethanol, or 75 μM blebbistatin (Sigma-Aldrich) in 0.0045% DMSO, for 30 min at 37°C where indicated, as previously described (16).

^{51}Cr release Cytotoxicity assay

Cytolytic activity was measured by ^{51}Cr release assay, and where specified, lytic units calculated as described (34). For cytotoxicity assay with isolated lytic granules, 3×10^6 cell equivalents of each density gradient fraction were washed and resuspended in PBS, then added to 1×10^4 ^{51}Cr–loaded 721.221 or KT86 target cells in HBSS along with 2 mM $CaCl_2$. To control for the protein contained in added granule fractions, target cells used for measuring the spontaneous release of ^{51}Cr were suspended in 0.03% BSA in PBS with 2 mM $CaCl_2$.

Fixed cell microscopy

Conjugates between NK and target cells at a 2:1 ratio were formed in suspension for 30 min and adhered to poly-L-lysine-coated glass slides (Polyprep, Sigma-Aldrich) for 15 min, all at 37°C, as described (7). Fixing, permeabilization, and staining were performed as previously (6), except the following reagents were used in the specified sequence: 1) anti-myosin IIA (Sigma) or rabbit IgG control (Sigma), or anti-myosin IIA (Abcam) or mouse IgG control; 2) anti-rabbit Pacific Blue (Molecular Probes) or anti-mouse Pacific Blue (Molecular Probes); 3) rabbit IgG (to block nonspecific binding); 4) unconjugated or FITC-conjugated anti-perforin clone ΔG9 (BD) or nonspecific IgG clone MOPC21 (BD, as a control); 5) Alexa Fluor 647-conjugated highly cross-adsorbed goat anti-mouse (Invitrogen), or AlexaFluor 647-conjugated phalloidin or 647-conjugated streptavidin control (Molecular Probes). All antibodies were used in the range of 0.6–20 μg/mL. Slides were covered with 0.15 mm coverslips (VWR Scientific) using mounting medium (Molecular Probes). Imaging was performed using a spinning disk confocal microscope (Olympus IX-81 DSU), and images analyzed using Volocity software (Improvision). For evaluation of myosin IIA, GFP, actin, and perforin localization throughout the cell volume, 20–30 images were acquired through the z-axis at 0.5 μm intervals and reconstructed using Volocity software.

In all experiments, detection settings were adjusted so that control-stained samples were uniformly negative and experimentally stained samples were not saturating or emitting signal detectable using filter sets intended for imaging other fluorophores. Settings were not adjusted throughout the experiment to allow for quantitative assessment of signals. The accumulation of fluorescent molecules was examined using the intensity threshold of 1.5–3.5 SD higher than the mean intensity of the fluorophore within the field. The area occupied by an accumulated fluorescence intensity was measured using this threshold, and the area of colocalization between different fluorescent molecules was determined by measuring the area containing two or more accumulated fluorophores. The percentage colocalized was determined by comparing the area of colocalization to the total area occupied by a certain fluorophore. Images shown have a similar intensity threshold applied for visualization as for analysis in order to facilitate the visualization of the fluorescent signal measured. Analysis of perforin polarization to the IS was performed as described previously for MTOC polarization (6), using perforin fluorescence in place of α-tubulin. Quantitative analysis of F-actin accumulation at the IS was performed as described previously (6), with the following modification: a series of 1 μm^2 regions were generated to cover the IS, and the mean F-actin intensity measured and multiplied by the area of F-actin determined by applying the same threshold to all areas sampled.

Live cell microscopy

NK cells were loaded with Lysotracker Red DND-99 (Molecular Probes), incubated for 30 min at 37°C, washed, and resuspended in RPMI with 10% FCS. KT86 or 721.221 target cells were adhered to a ΔT dish (Bioptechs) pre-coated with anti-CD48 (BD, for 721.221) or anti-CD58 (BD, for KT86) mAb for 30 min at 37°C. Lysotracker-loaded NK cells were introduced to the ΔT dish at a 1.5:1 effector to target ratio, and cells were imaged in a single z-plane using an Olympus IX-81 spinning disk confocal microscope and Volocity Software (Improvision) every 15 seconds over the course of 20–30 min of conjugation. Temperature was maintained at 37°C over the course of the experiment using ΔT dish heater and objective heater units (Bioptechs). For analysis of colocalization over time, 3–5 images were chosen from ≥8 conjugates which contained visible lytic granules and represented stages of IS formation (recognition of target cell, lytic granule clustering and initial polarization, final stages of granule polarization). Values were averaged with others representing similar time after conjugation binned by 1 min intervals. Accumulation of fluorescent molecules was analyzed as described above for fixed cells, using a similar intensity threshold to define accumulation of fluorescent signal. The area occupied by accumulated fluorescence was measured and the

percent colocalized area determined for each time point. Images shown have a similar intensity threshold applied for visualization as for analysis in order to facilitate the visualization of the fluorescent signal measured.

Total internal reflection fluorescence (TIRF) microscopy

4×10^5 YTS cells were loaded with 10 μM Lysotracker Green (Invitrogen), resuspended in 0.5 mL RPMI with 10% FCS, and added to anti-CD28 coated ΔT dishes (Bioptechs) heated to 37° C. Cells were imaged through the z-axis 25 min after addition, using confocal microscopy to identify cells with granules polarized to the anti-CD28-coated glass. Cells were then visualized using a 90° side port on the same microscope outfitted with a TIRF illuminator (Olympus) and an Argon 488nm laser (Melles Griot) with a 60x 1.45 NA objective. Images were acquired in TIRF mode at the interface between the cell and glass over 30s at a rate of 5 images/sec. Image streams were analyzed by cropping to the cell of interest, then further cropping to the cell footprint by applying an inclusive classifier to detect objects that fell above the mean intensity of the image. Objects within the cell having an intensity >3 SD above the mean intensity of all pixels and >0.05 μm^2 were included for analysis. Object tracks were identified over time using the Volocity Shortest Path tracking model set to join broken tracks with a maximum distance between objects of 0.05 μm. Objects not assigned to a track, i.e. those that were present for only one timepoint, were excluded from analysis.

Analysis of NK cell degranulation

PBMCs were resuspended at a concentration of 1×10^6 cells/mL to which 1×10^5 K562 cells, 3μg/mL anti-CD28 and anti-CD49d (BD Biosciences), 0.7 μg/mL monensin (BD Biosciences), 1 μg/mL brefeldin A (Sigma-Aldrich) and anti-CD107a were added. Cells were incubated at 37°C, 5% CO_2 for 5h, washed, stained for viability with Aqua amine-reactive viability dye (Invitrogen), and then stained with surface antibodies. K562 were not added to control samples. Antibodies for surface staining included anti-CD4 PE-Cy5-5 (Invitrogen) or PerCP-Cy5.5 (BD Biosciences), anti-CD56 PE (BD Biosciences) and anti-CD107a FITC (BD Biosciences). The cells were then washed and permeabilized using the Cytofix/Cytoperm kit (BD Biosciences) according to the manufacturer's instructions and stained with anti-CD3 Qdot 585 for 1 hour, washed, and fixed in PBS containing 1% paraformaldehyde. For each specimen, between 500,000 and 1,000,000 total events were acquired on a modified flow cytometer (LSRII; BD Immunocytometry Systems). Antibody capture beads (BD Biosciences) were used to prepare individual compensation tubes for each antibody used in the experiment. Data analysis was performed using FlowJo version 8.8.2 (TreeStar).

Western blot

For Western blotting of total lysate, cells were lysed in ice-cold lysis buffer (25 mM Tris-Cl, pH 7.5, 150 mM NaCl, 5 mM $MgCl_2$, 1% NP-40, 1 mM DTT, 5% glycerol). Proteins from 2.5×10^6 cell equivalents per sample were separated on a 4–12% Bis-Tris density gradient gel (Invitrogen) and transferred to nitrocellulose membranes (Invitrogen), which were blocked in 3% BSA and 140 mM NaCl Tris-buffered saline (TBS) and then incubated with anti-myosin IIA (Sigma) and anti-GFP (Santa Cruz) Ab. Bound antibodies were detected with anti-rabbit or anti-mouse IgG coupled to fluorophores (AlexaFluor 680, Molecular Probes; IRDye 800, Rockland), and imaged using the Odyssey Infrared Imaging System (Li-Cor Biosciences). For Western blotting of isolated lytic granules and related samples, $4–5.6 \times 10^5$ cell equivalents of density gradient fractions were separated and transferred as described above, and membranes were incubated with the following antibodies: anti-myosin IIA (Sigma M8064), anti-myosin IIA (Abcam 55456) anti-granzyme B (Sigma), anti-actin (Sigma), anti-perforin (Diaclone) or anti-LAMP-1 (BD Biosciences). The Sigma antibody to myosin IIA detects the C-terminus of the protein, while the Abcam antibody detects an internal epitope which is not truncated in the

1933x protein. Bound antibodies were detected as described above. Densitometric analysis was performed for Western blots using Li-Cor Odyssey software.

NK cell IFN-γ secretion

YTS NK cells were pre-incubated with blebbistatin or vehicle for 30 min at 37°C, after which media or 721.221 target cells at a 2:1 effector to target cell ratio were added for 0, 4, or 22 hours. After incubation, cell supernatants were removed and frozen at −80°C and then batch analyzed by IFN-γ ELISA (R&D Systems). For analysis of eNK IFN-γ secretion, eNK cells were pre-incubated with blebbistatin or vehicle, then incubated with 721.221 cells as described above for 22 hours.

Isolation of granules from NK cells

1–3 × 10^8 YTS or YTS-Myosin II-GFP NK cells were lysed and homogenized using a Dounce homogenizer. The homogenized lysates were subjected to centrifugation at 1000*g* to remove the nuclei. The postnuclear lysate (PNL) was subjected to centrifugation at 18,000*g* to pellet the lytic granules, yielding the crude lysosomal fraction (CLF). The CLF was resuspended in extraction buffer and subjected to density gradient ultracentrifugation at 150,000*g* on an 8–27% Optiprep gradient (Lysosomal Isolation Kit, Sigma-Aldrich, or Lysosome Enrichment Kit, Pierce). Fractions of 0.53 mL were harvested for further analysis. For isolation of lytic granules from human NK cells, 1 × 10^8 NK cells were isolated as described above from peripheral blood, and granule isolation was performed as described above. Where specified for comparison to conjugated cell granules, 2 × 10^8 YTS or YTS-Myosin IIA-GFP NK cells and 1 × 10^8 KT86 target cells were either incubated together at 37°C for 30 min before being lysed, or were lysed and homogenized separately, and then mixed. The lysates of both cell types were then subjected to the lytic granule isolation procedure described above.

Biotinylation of Isolated Lytic Granules

The lytic granule density gradient fraction found by Western blot to contain the most granzyme B and myosin IIA was washed in PBS and divided into two equal-volume portions. One portion was incubated with PBS pH 8.0 alone, while the second portion was incubated with EZ-Link Sulfo-NHS-SS-Biotin (Pierce) in PBS pH 8.0 at RT for 30 min following manufacturer's instructions. Both portions were then washed 2X with ice-cold PBS and lysed in 1% NP-40. Lysed granules were pre-cleared at 8200*g* for 10 minutes, then incubated with streptavidin-agarose beads (Millipore) at 4°C for 1 hour. Beads were pelleted at 8200*g*, then washed 3X with ice-cold PBS. Immunoprecipitated proteins were released from beads by boiling in LDS sample buffer (Invitrogen) and subjected to gel electrophoresis and Western blot as described above.

Serine Esterase Assay

Equal volumes of each lytic granule isolation density gradient fraction were placed into a 96-well plate, to which a substrate solution consisting of PBS containing 9.8 mM HEPES (Gibco), 196 μM N-a-Cbz-L-lysine thiobenzyl ester hydrochloride (BLT, Sigma) in 1:1 acetic acid:ethanol, and 218 μM 5,5′-dithiobis(2-nitrobenzoic acid) (DTNB, Sigma) in ethanol was added. Whole cell lysate from 1–2.5 × 10^5 YTS cells was added to separate wells as a control. Samples were incubated with substrate solution for 30 min at 37°C, and following incubation, absorbance was measured at 415 nm.

Actin-binding centrifugation assay

F-actin was generated from purified G-actin using standardized reagents (Cytoskeleton, Inc.) according to manufacturer's instructions and allowed to stabilize for 14 hours at 23°C. Isolated lytic granule samples from one fraction of the density gradient were incubated for 30 min at

23°C in the presence or absence of 3.83 μM F-actin. Actin bundling protein α-actinin was added at 20 μg/mL as a positive control. Samples were then precipitated by centrifugation at 18,000*g*, a force lower than needed to precipitate F-actin but suitable for precipitating lytic granules. The precipitate and supernatant were evaluated for the presence of actin and granzyme B by Western blot.

Actin-binding flow chamber assay

Purified G-Actin (11.5 μM, Cytoskeleton, Inc.) was polymerized using F-actin polymerization buffer (Cytoskeleton, Inc.) in the presence of 11 μM unlabeled phalloidin (Sigma-Aldrich), 0.85 μM biotinylated phalloidin (Molecular Probes), and 1.41 μM Alexa Fluor 647-labeled phalloidin (Molecular Probes), then allowed to stabilize for 4 hours at 23°C. 50 mm coverslips (VWR) were coated with 10 μg/mL biotinylated BSA (Pierce), followed by 10 μg/mL streptavidin (Jackson ImmunoResearch), and where specified, followed by polymerized, phalloidin-stabilized F-actin. A flow chamber was created by adhering a 40 mm coverslip (VWR) to each protein-coated coverslip using silicone grease. 150 μL of isolated lytic granules from a density gradient fraction enriched in myosin IIA and granzyme B were washed in PBS at 18,000*g*, incubated with Lysotracker Red DND-99 for 30 min at 37°C, washed, and resuspended in physiologic salt buffer (25 mM KCl, 2 mM $MgCl_2$, 20 mM HEPES pH 7.6). Where specified, granules were also incubated with and maintained in 75 μM blebbistatin. Lytic granules were added to the flow chamber dropwise, and buffer drawn through the chamber using Whatman paper at the opposite end. After granules had adhered to the slide despite continued buffer flow, high-salt/ATP (100 mM KCl, 2 mM $MgCl_2$, 20 mM HEPES, pH 7.6, 5 mM ATP) solution was added to the chamber. Granules were allowed to flow through or adhere to the chamber for 1–2 minutes before imaging with an Olympus IX-81 spinning disk confocal microscope at maximum speed (approximately 5 images/sec). Images were analyzed using Volocity software, in which granules were defined as objects containing 2 SD or higher GFP intensity (for Myosin IIA-GFP cell granules) or Lysotracker Green intensity (for human NK granules). Objects less than 1 μm^2 in area were excluded as debris. The “Track Objects” function in Volocity was used following the “Shortest Path” tracking model, identifying moving objects as tracks. Broken tracks were joined by the program using a maximum distance between objects of 20 μm to avoid identifying one moving granule as multiple tracks, and to allow accurate joining of fast-moving objects. Tracks with displacement greater than 5 μm were considered to be lytic granules in motion in the flow chamber, and were counted, then divided by the duration of the video to control for differences in imaging time. For visualization of BSA/SA- and BSA/SA/Actin-coated flow chambers, separate flow chambers were made containing BSA/SA or BSA/SA and F-actin, stabilized with 11 μM AlexaFluor 488-labeled phalloidin (Molecular Probes). Flow chambers were visualized by TIRF microscopy as described above.

Mass spectrometry

Fractions of the lytic granule density gradient shown by Western blot to be enriched in granzyme B and myosin IIA were separated by electrophoresis on a 4–12% Bis-Tris density gradient gel (Invitrogen) which was stained with colloidal Coomassie. Individual bands of interest were excised, digested with trypsin, and subjected to vacuum matrix-assisted laser desorption (vMALDI) mass spectrometry as described (21) in the Stokes Protein Core Facility of the Children’s Hospital of Philadelphia. MS data was analyzed using Scaffold software (Proteome Software Inc).

Electron microscopy (EM)

200 μL of isolated lytic granules from YTS NK cells was washed in PBS at 18,000*g* and resuspended in 1 mL of immuno-EM fixative (4% paraformaldehyde, 0.1% glutaraldehyde,

0.1 M sodium cacodylate buffer pH 7.4) for 18 hours at 4°C. After subsequent dehydration in ethanol, the sample was embedded in L.R. White resin and polymerized with UV light at −20° C. Ultrathin sections on nickel grids were treated with a blocking solution containing ovalbumin and cold water fish skin gelatin prior to incubation with anti-myosin IIA antibody (Sigma). After multiple PBS washes, sections were treated with a goat anti-rabbit secondary antibody conjugated to 6 nm gold particles. Sections were imaged in the Biomedical Imaging Core Facility of the University of Pennsylvania using a JEOL 1010 electron microscope fitted with a Hamamatsu digital camera system. True immunogold labeling in images was identified using AMT imaging software by reducing gamma to 0.3. Data shown, however, represent the original unmodified image.

Statistics

For fixed and live cell microscopy, the minimum number of cells evaluated in a given experiment was determined using a sample size calculation based upon preliminary data, with α and β error levels of 1%. For statistical analyses, differences between cell types or conditions were determined using an unpaired two-tailed Student's *t* test or an exact Wilcoxon-Mann-Whitney test. Differences were considered significant if $p<0.05$.

RESULTS

Human NK cells with a myosin IIA 1933x mutation have reduced cytotoxicity and lytic granule entry into F-actin at the IS

Inhibition of myosin IIA with blebbistatin or ML-9, or reduction of its expression using siRNA was previously shown to block NK cell cytotoxicity but not lytic granule polarization to the IS (16). Thus, we wanted to determine the role of myosin IIA in enabling granule release following lytic granule polarization. To evaluate an endogenous role for myosin IIA in human NK cells with a link to disease, we assessed NK cell function in four May-Hegglin anomaly patients heterozygous for a C5797T mutation in MYH9. This mutation introduces a stop codon leading to C-terminal truncation of the myosin IIA heavy chain at position 1933 (1933x (30, 32)). PBMCs from all four patients demonstrated significantly reduced cytotoxic activity against K562 target cells when compared to control donors (Fig. 1A,B). To determine that the reduction in cytotoxicity was not transient, one of the four patients (patient 1) was evaluated longitudinally. In four independent assessments over a period of twenty months, the mean cytotoxicity mediated by patient PBMCs was reduced (data not shown). To ensure that the reduced cytotoxicity was not a feature of other cells present in PBMC preparations, and to control for potential variability in the percentage of NK cells, NK cells from three patients and controls were enriched by negative selection and immediately evaluated in a cytotoxicity assay. The cytotoxic activity of patient ex vivo NK (eNK) cells against K562 target cells was still reduced compared to control eNK cells (Fig. 1B, C). Since myosin IIA was previously shown to be needed for NK cell degranulation as determined by CD107a upregulation (16), we wanted to determine if the decreased cytotoxicity in patient NK cells was due to a similar blockade. After incubation with K562 target cells, CD107a was upregulated on control donor NK cells, but not on those from a patient (Fig. 1D). Thus, both cytotoxicity and degranulation are defective in patients with a myosin IIA truncation, similar to blebbistatin or MYH9 siRNA-treated NK cells (16).

To examine the mechanism underlying defective cytotoxicity in 1933x patient NK cells, we evaluated the localization of perforin, which is contained in lytic granules, relative to F-actin and myosin IIA at the IS in patient eNK cells. Control donor and 1933x patient eNK cells were conjugated to K562 target cells, fixed, and evaluated using confocal microscopy. In eNK cells with perforin polarized toward the IS, volumes of perforin, actin, and myosin IIA fluorescence were identified. In control eNK cells, there was extensive colocalization between volumes of

perforin and F-actin (Fig. 2A,F and Supplementary Video 1A) suggesting the penetration of lytic granules into accumulated F-actin at the IS. In contrast, in 1933x eNK cells (Fig. 2B,G and Supplementary Video 1B) and blebbistatin-treated eNK cells (Fig 2C and Supplementary Video 1C), perforin was polarized toward the IS (quantified in Fig. S1A), but there was substantially reduced colocalization between volumes of perforin and F-actin at the IS compared to control (Fig. 2E,I). This suggests that myosin-IIA function was required for lytic granule penetration into F-actin accumulated at the IS.

To begin to understand the role of myosin IIA in granule penetration into F-actin at the IS, we evaluated myosin IIA localization in eNK cells using one of two different antibodies. The first detected only wild-type myosin IIA, while the second detected both truncated and wild-type forms. In control eNK cells, there was extensive colocalization between perforin and myosin IIA (Fig. 2A,D,E,F,H,I and Supplementary Video 1D). In patient eNK cells, colocalization between perforin and wild-type myosin IIA was reduced (Fig. 2B,D,E, S1C,D and Supplementary Video 1E), but when total myosin IIA was considered, the colocalization of perforin with myosin IIA was similar to control (Fig. 2G,H,I). This suggests that although a normal amount of myosin IIA colocalized with perforin in patient NK cells, its function was reduced by the inclusion of the mutant form. In blebbistatin-treated eNK cells, however, the colocalization between perforin and myosin IIA was slightly reduced compared to control (Fig. 2C,D,E and Supplementary Video 1F). Differences were not a feature of protein present per unit volume, as the total mean intensity of fluorescent regions was similar between the different eNK evaluated (Fig. S1B). The quantity of perforin and actin in cells and the quantity of F-actin accumulated at the IS was also similar between control, 1933x, and blebbistatin-treated cells (Fig. S1A–B, S1G), suggesting that defective myosin IIA was not affecting these parameters. Thus, although actin accumulated at and perforin polarized toward the IS, the colocalization between perforin and F-actin in 1933x and blebbistatin-treated eNK cells was reduced relative to control. This suggests decreased penetration of lytic granules into the F-actin cortex at the IS in these cells and implies a role for myosin IIA in facilitating lytic granule interaction with F-actin after they are polarized to the IS.

Myosin IIA is not required for IFN-γ secretion

Because myosin IIA was previously demonstrated to be necessary for exocytosis of lytic granule contents (16), we wanted to determine whether it is a general requirement for all types of secretion in NK cells. Thus, we measured IFN-γ secretion, which is a differentially regulated process from degranulation in NK cells (35). We initially used YTS NK cells because they require myosin IIA for cytotoxicity and lytic granule release, similar to eNK cells (16). YTS cells were treated with vehicle control or blebbistatin and incubated in the presence or absence of 721.221 target cells. The secretion of IFN-γ into the supernatant was determined by ELISA after 0, 4, or 22 hours of incubation. In the absence of 721.221 cells, there was minimal IFN-γ in both vehicle- and blebbistatin-treated cell cultures. In the presence of 721.221 cells, however, IFN-γ secretion was augmented after 4 hours and increased further after 24 hours of incubation. The amount of IFN-γ secreted by blebbistatin-treated cells was similar to that secreted by vehicle-treated cells (Fig. 3A). This result was extended to control donor eNK cells allowed to conjugate with 721.221 cells, where there was also no inhibition of IFN-γ secretion observed in blebbistatin-treated relative to vehicle-treated cells (Fig. 3B). This demonstrates that myosin IIA is not required for cytokine secretion, and that it is not a generalized requirement for secretory activity in NK cells.

Myosin IIA and perforin colocalize in NK cells before and throughout IS formation

Because the requirement for myosin IIA in secretion appears to be specific to NK cell lytic granule contents, we wanted to more thoroughly evaluate the localization of myosin IIA relative to lytic granules in NK cells. YTS cells expressing a myosin IIA-GFP fusion protein (YTS-

MyoIIA-GFP) were generated and compared to YTS cells expressing GFP alone using fixed and live cell confocal microscopy. Both of these cell lines, as well as parental YTS cells, expressed similar levels of endogenous myosin IIA (Fig. S2A), however, YTS-MyoIIA-GFP cells expressed the additional myosin IIA-GFP fusion protein. The overexpression of myosin IIA in these cells did not alter their cytotoxic function, as measured in ^{51}Cr-release assays (Fig. S2B–C).

Using these cells, we first determined the localization of myosin IIA and perforin throughout their volumes when conjugated to K562 cells made susceptible to YTS cell cytotoxicity by stable expression of CD86 (KT86 (6)). As myosin IIA is abundant in NK cells, an analysis algorithm was used with an intensity threshold to include only the most intense fluorescent signal for myosin IIA, GFP, and perforin. Myosin IIA was cytoplasmic but demonstrated variations in intensity, as identified using anti-myosin IIA antibody, in fixed conjugates from all three cell lines (Fig. 4A–C). In YTS-GFP cells, GFP was localized throughout the cells, while in YTS-MyoIIA-GFP cells, the GFP resembled myosin IIA localization (Fig. 4B–C), and the mean percent colocalization between GFP and myosin IIA in YTS-MyoIIA-GFP cells was higher than in YTS-GFP cells (Fig. S3A). Thus, myosin IIA-GFP fusion protein but not GFP alone recapitulated the localization of endogenous myosin IIA.

In all cell lines, myosin IIA colocalized with lytic granules, as 4–14% of the myosin IIA volume colocalized with perforin, and 39–65% of perforin volume colocalized with myosin IIA (Fig. S3B). Thus, a small pool of myosin IIA localized in lytic granule regions, but a large proportion of lytic granule regions colocalized with myosin IIA. A similar colocalization between perforin and myosin IIA-GFP fusion protein, but not GFP alone, was identified in YTS-MyoIIA-GFP and YTS-GFP cells, respectively (Fig. S3A). Thus, the localization of the myosin IIA-GFP fusion protein to lytic granule regions was specific.

We next wanted to determine if the colocalization between myosin IIA and lytic granules changed during NK cell activation and IS formation in living cells. YTS-MyoIIA-GFP or YTS-GFP cells were loaded with Lysotracker Red dye to visualize the lytic granules, added to environmental chambers containing KT86 target cells and imaged every 15 seconds. After conjugation, the lytic granules in NK cells began to polarize toward the target cell (Fig. 4D–E). During this time, in YTS-MyoIIA-GFP cells, a portion of the myosin IIA-GFP in the cell remained with the lytic granules and polarized along with them toward the IS (Fig. 4D and Supplementary Video 2). Although lytic granules still polarzed to the IS in YTS-GFP cells, the GFP was not increased in the region of the lytic granules (Fig. 4E and Supplementary Video 3). This dynamic localization of myosin IIA-GFP, but not GFP alone, with lytic granule regions was best visualized using a GFP intensity pseudocor scale (Fig 4D,E bottom and supplementary videos 2,3 bottom). To quantify this colocalization, multiple conjugated and unconjugated YTS-MyoIIA-GFP cells were compared, and only the most intense myosin IIA-GFP fluorescence was measured (>1.5 SD above the mean fluorescence intensity). The colocalization of Lysotracker Red with myosin IIA-GFP was similar in unconjugated (mean = 65±4%) and conjugated (mean = 77±10) cells with no specific trend toward an increase or decrease in colocalization (Fig. 4F). A similar consistent colocalization between cellular myosin IIA-GFP and Lysotracker Red was identified (12±1 in unconjugated and 17±4 in conjugated cells) (Fig. 4G). Furthermore, the intensity of myosin IIA-GFP within Lysotracker Red regions remained constant after conjugation (Fig. 4H), suggesting that recruitment of myosin IIA-GFP to lytic granules was unlikely. The colocalization between Lysotracker Red and GFP in YTS-GFP cells was consistently lower than in YTS MyoIIA-GFP cells (Fig. 4I), thus demonstrating that the presence of myosin IIA in the GFP fusion enabled its preferential and consistent colocalization with lytic granules.

Myosin IIA is associated with NK cell lytic granules

To biochemically determine if myosin IIA interacts with lytic granules, granules were isolated from NK cells by density gradient separation and collected in seven equal volume fractions. Myosin IIA was identified in the lytic granule preparation by Western blot, and co-migrated with perforin, granzyme B, and LAMP-1 (Fig. 5A). All four proteins were enriched in fractions 4–6 compared to the post nuclear lysate. These fractions contained 80–90% of the total protein in the granule fractions. There was a paucity of actin in lytic granule fractions, demonstrating the general lack of cellular contamination (Fig 5A). Myosin IIA-containing lytic granule fractions possessed granzyme A activity (Fig. 5B) and were able to kill ^{51}Cr-labeled KT86 and 721.221 target cells (Fig. 5C–D). The presence of myosin IIA in these fractions was verified by mass spectrometry, as were perforin and granzyme B (Fig. 5E and data not shown). This association was also observed by confocal microscopy. Lytic granules isolated from YTS-MyoIIA-GFP cells and loaded with Lysotracker Red demonstrated red and green fluorescence in granule-sized organelles (Fig. 5F). The association between myosin IIA and lytic granules did not change after target cell conjugation, as granules prepared from unconjugated and conjugated YTS cells had a similar amount of myosin IIA when compared to the amount of granzyme B by Western blot analysis (Fig. S4).

To ensure that our results were not specific to YTS cells and to determine if 1933x myosin IIA affected interaction with lytic granules, granules were isolated from control donor and patient culture-propagated NK cells. In both normal donor and patient lytic granules, myosin IIA co-migrated with granzyme B (Fig. 5G,I) and with granzyme A activity (Fig. 5H,J), implying that myosin IIA associates with human NK cell lytic granules. To determine if the mutant myosin IIA was capable of interacting with lytic granules, we utilized the two different myosin IIA antibodies used in Fig 2. If only wild-type myosin IIA were associated with lytic granules, the densitometric ratio of bands detected with the two different antibodies should approach 1.0. As expected, this ratio approximated 1 in control donor lytic granules (Fig. 5G), but did not in patient lytic granules (Fig. 5I). Thus, both wild type and mutant myosin IIA was associated with lytic granules from patient NK cells. The densitometric ratio of total myosin IIA to granzyme B was similar in patient and control lytic granules, however, and therefore the total quantity of myosin IIA was not reduced in patient granules compared to control (Fig. 5G,I).

To gain greater insight into how lytic granule-associated myosin IIA could contribute to function, we next attempted to determine the precise localization of myosin IIA on NK cell lytic granules. We first performed immuno-electron microscopy on intact unconjugated control donor eNK cells as well as isolated YTS cell lytic granules. In unconjugated eNK cells, myosin IIA was identified on the periphery of lytic granules (Fig. 6A). This was confirmed by EM analysis of isolated lytic granules, which were decorated with anti-myosin IIA antibody (Fig. 6B), but not secondary antibody alone (Fig. 6C). As an additional approach, isolated lytic granules were surface biotinylated, followed by precipitation of granule surface proteins with streptavidin-agarose. Here, myosin IIA was identified in the precipitate from biotinylated lytic granules, but not unlabeled lytic granules (Fig. 6D). Overall, these data suggest that myosin IIA is associated with lytic granules in NK cells and is located on their surface and not in the core of these organelles. In this location, it may be poised to facilitate the interaction of lytic granules with actin and their penetration into the F-actin-rich IS.

Myosin IIA-associated lytic granules can bind F-actin

To demonstrate a potential function of lytic granule-associated myosin IIA, we examined the ability of isolated NK cell lytic granules to bind F-actin using a centrifugation-based assay. Lytic granules were incubated in the presence of F-actin and then subjected to centrifugation at a speed which pellets lytic granules, but not F-actin alone. Addition of YTS cell lytic granules to F-actin resulted in the presence of F-actin in the lytic granule pellet and reduced F-actin in

the residual supernatant (Fig. 7A,B). The percent of F-actin pelleted by the lytic granules was similar to that obtained in the pellet after addition of the actin bundling protein α-actinin, which was used as a positive control to aggregate F-actin. Transmission EM of the pellet from lytic granules added to F-actin demonstrated filamentous material associated with the lytic granules (Fig. 7E); the granule pellet alone without added F-actin did not (Fig. 7F). Similarly, Western blot of the granule pellet from the control portion of this assay, in which F-actin was not added, did not demonstrate the presence of actin (Fig. 7A). Thus, the presence of actin in the pellet after addition of exogenous F-actin defines a specific interaction between lytic granules and F-actin.

To confirm that this property of NK cell lytic granules was not specific to YTS cells, and to evalute the effect of 1933x myosin IIA, F-actin-binding assays with isolated lytic granules from control donor and patient NK cells were performed. The addition of control, but not patient, NK cell lytic granules to F-actin resulted in actin in the lytic granule pellet and reduced actin in the residual supernatant (Fig. 7C,D). Overall, while control donor NK cell lytic granules were able to associate with nearly the same amount of F-actin as the positive control (86±2% of the quantity removed from the supernatant by α-actinin determined by densitometry of actin bands), granules from 1933x patient NK cells could only associate with less than half of the amount of F-actin as positive control (42±3% of α-actinin). This demonstrates that normal human NK cell lytic granules can bind F-actin and suggests that 1933x myosin IIA reduced the ability of patient lytic granules to interact with F-actin. This implies a specific role for lytic granule-associated myosin IIA in F-actin binding.

To directly observe the binding of the isolated lytic granules to F-actin, we constructed microflow chambers coated with biotinylated BSA and streptavidin (BSA/SA, Fig. S5), or BSA/SA and F-actin stabilized with biotinylated phalloidin (Fig. S5), to which lytic granules were added. We initially studied lytic granules from YTS-MyoIIA-GFP cells, which were visible by confocal fluorescence microscopy due to the presence of myosin IIA-GFP. When suspended in a physiologic salt buffer and added to a BSA/SA-coated microflow chamber, the lytic granules did not adhere to the coated glass surface (Fig. 8A,B and Supplementary Video 4A). When added to an F-actin-coated microflow chamber, however, the granules adhered to the chamber, despite continued flow of buffer (Fig. 8A,B and Supplementary Video 4B). After lytic granules were stable in their position, buffer was changed from physiologic salt to high salt containing 5 mM ATP, which abrogates myosin II binding to F-actin by first causing myosin II detachment from actin through its ATP-dependent motor activity and then preventing rebinding through the presence of high salt (36). Under these conditions, most granules no longer adhered to the microflow chamber (Fig. 8A,B and Supplementary Video 4C). The granules did not begin to move through the chamber upon addition of high-salt buffer containing no ATP (data not shown), suggesting that the granules are released from F-actin by the addition of ATP. Granules that were pretreated with blebbistatin also failed to properly adhere to F-actin-coated chambers (Fig 8A), further implicating a specific role for myosin II.

To confirm that these properties of YTS-MyoIIA-GFP-derived lytic granules were relevant to primary human NK cells and to define the effect of 1933x myosin IIA, lytic granules prepared from culture-propagated control and patient eNK cells were loaded with Lysotracker Green and evaluated in the microflow chambers. In F-actin-coated chambers with physiologic salt buffer, control, but not patient, granules adhered to the coated glass surface similarly to the YTS-MyoIIA-GFP granules (Fig. 8C,D and Supplementary Videos 5A,6A). Upon exposure to high-salt buffer containing ATP, granules from both control donor and patient eNK cells were not adherent to the F-actin-coated chamber (Fig. 8C,D and Supplementary Videos 5B, 6B). These results demonstrate a direct interaction between NK cell lytic granules and F-actin and suggest a critical role for intact myosin IIA function in this process.

Myosin II function is necessary for lytic granule approach to the IS

Since we found that NK cell lytic granules adhere to F-actin, we wanted to determine if myosin IIA could facilitate granule movement through the F-actin dense cell cortex. To test this, we used TIRF microscopy to image granules at the activated surface of YTS cells. We have previously shown that YTS cells polarize their lytic granules to and accumulate F-actin at anti-CD28-coated glass surfaces within 30 minutes (6). Thus, Lysotracker Green-loaded YTS cells were adhered to anti-CD28-coated environmental chambers for 25 minutes, and lytic granule polarization toward the contact site was determined using confocal fluorescent *z*-axis sectioning (Fig. 9A). Cells with polarized lytic granules were then imaged in TIRF mode at a maximum acquisition rate for 30 seconds. In control YTS cells, lytic granules were dynamically evident in the zone of TIRF illumination (Fig. 9A and Supplementary Video 7A). To evaluate a role for myosin II in this activity, YTS cells were pretreated with the myosin light chain kinase inhibitor ML-9, which inhibits myosin II function (29). ML-9 was used in this capacity for TIRF applications due to the phototoxicity of blebbistatin at 488 nm (37). ML-9-treated cells still polarized lytic granules toward the antibody-coated glass (Fig. 9A), but there were fewer lytic granules in the zone of TIRF illumination. Furthermore, the lytic granules which were apparent were less dynamic (Fig. 9A and Supplementary Video 7B).

To quantify the effect of ML-9 treatment on lytic granule dynamics, individual lytic granules from multiple control and ML-9-treated cells were identified, measured, and tracked throughout the duration of imaging. In control cells, granule area fluctuated over time, suggesting that granules were constantly moving toward and away from the NK cell membrane. In ML-9-treated cells, however, granule area was generally small and remained constant throughout imaging (Fig. 9B,C). Relative to control, ML-9-treated cells had a lower mean number of lytic granule tracks (Fig. 9D), which had less velocity, track length, total displacement and rate of displacement (Figs. 9D,F,H,I). The mean duration of each track was not different between control and ML-9-treated cells (Fig. 9G). Thus, lytic granule approach to and movement at the IS is diminished by ML-9 treatment. This suggests a critical role for myosin II in this prefinal step in NK cell cytotoxicity, where lytic granules traverse the cell cortex to reach the NK cell plasma membrane.

DISCUSSION

NK cell cytotoxicity occurs largely through the directed exocytosis of lytic granule contents onto target cells. Previously, myosin IIA was shown to be dispensable for NK cell conjugation with target cells, IS formation, and lytic granule polarization towards the IS, but required for degranulation (16). Here, using NK cells from four patients with a mutation in myosin IIA, we identify a mechanism for myosin IIA function in NK cells. Specifically, myosin IIA associates with lytic granules and enables their interaction with F-actin as well as their final approach to the IS.

This function of myosin IIA is likely critical, as there is a substantial accumulation of F-actin at the IS, which could prevent a large organelle such as a lytic granule (up to 1 μm in diameter (38)) from reaching the cell membrane. Clearances in cortical actin have been identified at the secretory domain in CTLs (39) and subsequently in NK cells (40). It was unclear, however, whether lytic granules require assistance in navigating a course through the actin cortex surrounding the secretory domain once they have reached the IS. In our studies of myosin IIA 1933x patient or blebbistatin-treated NK cells, we have found diminished colocalization between perforin and F-actin at the IS (Fig. 2), suggesting that functional myosin IIA is necessary for lytic granule penetration into the F-actin cortex at the IS. Myosin IIA is unlikely to function at the lytic IS in large-scale restructuring of F-actin, as overall F-actin organization at the IS was previously reported as normal in blebbistatin-treated cells (16), although minor contributions of myosin IIA at the IS in readjusting the actin cortex cannot be excluded.

In the present work, we found that myosin IIA was directly and constitutively associated with lytic granules using several techniques (Figs. 2,4,5). Although we identified myosin IIA in lytic granule preparations in both YTS and donor-derived NK cells (Fig 5), it is possible that myosin IIA was present in these preparations due to an association with organelles of similar density to lytic granules. This is unlikely, however, as myosin IIA was visualized with isolated lytic granules by confocal microscopy (Fig. 5) and was at the periphery of lytic granules in ultrastructural analyses of intact eNK cells and isolated lytic granules (Fig. 6). Localization at the periphery of these organelles is important because this would allow myosin IIA to serve a functional role on intact granules. The constitutive association of myosin IIA with lytic granules (Fig. 4,5 and S4) suggests that myosin IIA is unlikely to be recruited to lytic granules upon NK cell activation, although rapid turnover of granule-associated myosin IIA cannot be excluded. The association of myosin IIA with lytic granules would be akin to the functions of certain myosin isoforms in other cell types. Examples include myosin V (reviewed in (41)) and myosin II (42–47), which are implicated in vesicle transport. Myosin IIA, specifically, has also been linked to degranulation in mast cells (17,48), although it is unclear whether myosin IIA is associated with mast cell granules or is involved in remodeling the cytoskeleton in these cells. Our findings expand upon the role of myosin IIA in organelle transport, indicating a specialized and direct role for myosin IIA in the transport of NK cell lytic granules.

The association of myosin IIA molecules to lytic granules could potentially occur directly through the granule membrane. The C-terminal fragment of myosin IIA can bind to phosphatidylserine-containing vesicles (49,50), and this property could enable a similar association with lytic granules. Alternatively, myosin IIA may associate with lytic granules in an indirect fashion, as demonstrated by the cooperative binding of myosin V with rab27a and melanophilin to melanosome membranes (51). Since myosin IIA has been previously identified in NK cells to exist in a complex with WIP and WASp (21), and WIP has been identified in NK cell lytic granule preparations (52), myosin IIA could potentially associate with lytic granules through this complex.

The specific association of myosin IIA with lytic granules may point to an inherent ability of lytic granules to reach the cell membrane once delivered to the cortex. Myosin IIA-associated lytic granules isolated from NK cells are capable of adhering to F-actin, even under the force of flow (Fig. 8). The sensitivity of this interaction to ATP and high salt implies that the protein or proteins responsible are regulated by ATP, a known property of myosins. There is a possibility that other actin-binding proteins associated with the granules may stabilize this interaction, but additional ATP-dependent actin-binding motor proteins were not identified in our proteomic analysis of lytic granule contents (data not shown), or in those published by others (53). A role for myosin IIA in the final approach of lytic granules to the IS was further identified in ML-9-treated NK cells using TIRF microscopy (Fig. 9), despite the fact that granule polarization occurred (Fig 9A), as previously demonstrated (16). This implies a role for myosin IIA in transporting lytic granules to the plasma membrane following their delivery to secretory domains at the IS. This function is likely to be specific for lytic granules, as IFN-γ secretion was not affected in blebbistatin-treated cells (Fig. 3), a distinction further supported by studies defining differential regulation of degranulation and IFN-γ production in NK cells (35,54).

The role for myosin IIA in NK cell lytic granule function was additionally demonstrated by NK cells from rare patients with May-Hegglin Anomaly due to a 1933x mutation in myosin IIA. Patient NK cells had defective cytotoxic activity and lytic granules which poorly colocalized with F-actin (Fig. 1), again suggesting that functional myosin IIA may be necessary for lytic granule entry into F-actin at the cell cortex. While one of the four patients we evaluated had an atypical infection (with *Listeria*) which has been shown to involve NK cell-mediated defense (55), it is presently unclear if this defect is of clinical significance due to the small

number of patients available for study with this mutation. A more comprehensive clinical assessment of patients with this particular, as well as other, MYH9 mutations is warranted.

The 1933x mutation affects the domain of myosin IIA involved in filament formation and cargo binding (49). It does not prevent formation of heavy chain dimers, but does result in abnormal bipolar myosin IIA filaments (56). These potential effects of myosin IIA 1933x in filament formation and/or cargo binding suggest two different mechanisms of how myosin IIA associates with lytic granules. First, myosin IIA could form bipolar filaments which wrap around lytic granules. In this case, the presence of the 1933x mutant in myosin IIA heterohexamers would alter filament structure and reduce F-actin binding capabilities, potentially due to poor filament contractility. Our data demonstrate that the quantity of myosin IIA associated with lytic granules is normal in patient NK cells (Fig. 5), but the function in interacting with F-actin is decreased (Fig 7,8). As a second potential mechanism, several myosin IIA molecules could associate with NK cell lytic granules in single hexameric units. Although one independent myosin IIA unit would have minimal processivity, multiple molecules could cooperate to enable granule interaction with F-actin (57). Single myosin IIA units attached to granules might lead to the directional rolling of granules along F-actin, while myosin IIA filament-wrapped granules might predict more random dynamics of individual granules. Further studies defining these interactions hold the potential to identify novel mechanisms of myosin IIA function.

Regulation of myosin IIA could also represent an important means for controlling lytic granule interaction with F-actin, and may be affected by the 1933x mutant myosin. A casein kinase II phosphorylation site exists at S1943 of the myosin IIA heavy chain (58), and is removed by the 1933x mutation. Additionally, PKC-mediated phosphorylation of S1916 (59,60) could be altered in the 1933x protein, as interaction of PKC with myosin IIA may be stabilized by the C-terminus of the protein. Regulation of myosin IIA through C-terminal phosphorylation has been established in murine T cells (15), suggesting that mutations disrupting phosphorylation sites may alter immunologic functions. The 1933x mutation may also affect interactions with mts1/S100A4, which is known to bind between residues 1909–1937 of myosin IIA and regulate myosin IIA phosphorylation states (61). Alterations in myosin IIA phosphorylation state could result in decreased function in binding to or movement across F-actin.

In cytotoxic lymphocytes, lytic granules are brought to the secretory domain by the MTOC, which approximates the cell membrane in cytolytic conjugates (4). Myosin IIA may facilitate the final transport of NK cell lytic granules through the F-actin cortex at the IS. Given that NK cells maintain abundant lytic granules at rest, this mechanism of tight control may be warranted. Additional identification of how myosin IIA is regulated to promote lytic granule exocytosis may therefore uncover important controls for NK cell cytotoxicity. The constitutive and functional association of myosin IIA with lytic granules, however, defines a critical requirement for accessing NK cell activity.

Supplementary Material

Refer to Web version on PubMed Central for supplementary material.

Acknowledgments

We thank Lynn Spruce and Steven Seeholzer for assistance with mass spectrometry; Raymond Meade and Neelima Shah for assistance with electron microscopy; Max Krummel, Michael Ostap, Jan Burkhardt, Jim Bussel, Alison Beal, and Huaqing Zhao for valuable discussions; Adam Dachis for assistance with video compilation; and Emily Williams, Kim Jordan, and Vikram Palanivel for early experimental directions.

References

1. Vivier E, Tomasello E, Baratin M, Walzer T, Ugolini S. Functions of natural killer cells. Nat Immunol 2008;9:503–510. [PubMed: 18425107]
2. Davis DM, Dustin ML. What is the importance of the immunological synapse? Trends Immunol 2004;25:323–327. [PubMed: 15145322]
3. Orange JS. Formation and function of the lytic NK-cell immunological synapse. Nat Rev Immunol. 2008
4. Stinchcombe JC, Majorovits E, Bossi G, Fuller S, Griffiths GM. Centrosome polarization delivers secretory granules to the immunological synapse. Nature 2006;443:462–465. [PubMed: 17006514]
5. Peters PJ, Borst J, Oorschot V, Fukuda M, Krahenbuhl O, Tschopp J, Slot JW, Geuze HJ. Cytotoxic T lymphocyte granules are secretory lysosomes, containing both perforin and granzymes. J Exp Med 1991;173:1099–1109. [PubMed: 2022921]
6. Banerjee PP, Pandey R, Zheng R, Suhoski MM, Monaco-Shawver L, Orange JS. Cdc42-interacting protein-4 functionally links actin and microtubule networks at the cytolytic NK cell immunological synapse. J Exp Med 2007;204:2305–2320. [PubMed: 17785506]
7. Orange JS, Harris KE, Andzelm MM, Valter MM, Geha RS, Strominger JL. The mature activating natural killer cell immunologic synapse is formed in distinct stages. Proc Natl Acad Sci U S A 2003;100:14151–14156. [PubMed: 14612578]
8. Kupfer A, Mosmann TR, Kupfer H. Polarized expression of cytokines in cell conjugates of helper T cells and splenic B cells. Proc Natl Acad Sci U S A 1991;88:775–779. [PubMed: 1825141]
9. Chen X, Allan DS, Krzewski K, Ge B, Kopcow H, Strominger JL. CD28-stimulated ERK2 phosphorylation is required for polarization of the microtubule organizing center and granules in YTS NK cells. Proc Natl Acad Sci U S A 2006;103:10346–10351. [PubMed: 16801532]
10. Kopcow HD, Allan DS, Chen X, Rybalov B, Andzelm MM, Ge B, Strominger JL. Human decidual NK cells form immature activating synapses and are not cytotoxic. Proc Natl Acad Sci U S A 2005;102:15563–15568. [PubMed: 16230631]
11. Feldmann J, Callebaut I, Raposo G, Certain S, Bacq D, Dumont C, Lambert N, Ouachee-Chardin M, Chedeville G, Tamary H, Minard-Colin V, Vilmer E, Blanche S, Le Deist F, Fischer A, de Saint Basile G. Munc13-4 is essential for cytolytic granules fusion and is mutated in a form of familial hemophagocytic lymphohistiocytosis (FHL3). Cell 2003;115:461–473. [PubMed: 14622600]
12. Menager MM, Menasche G, Romao M, Knapnougel P, Ho CH, Garfa M, Raposo G, Feldmann J, Fischer A, de Saint Basile G. Secretory cytotoxic granule maturation and exocytosis require the effector protein hMunc13-4. Nat Immunol 2007;8:257–267. [PubMed: 17237785]
13. Menasche G, Pastural E, Feldmann J, Certain S, Ersoy F, Dupuis S, Wulffraat N, Bianchi D, Fischer A, Le Deist F, de Saint Basile G. Mutations in RAB27A cause Griscelli syndrome associated with haemophagocytic syndrome. Nat Genet 2000;25:173–176. [PubMed: 10835631]
14. Bryceson YT, Rudd E, Zheng C, Edner J, Ma D, Wood SM, Bechensteen AG, Boelens JJ, Celkan T, Farah RA, Hultenby K, Winiarski J, Roche PA, Nordenskjold M, Henter JI, Long EO, Ljunggren HG. Defective cytotoxic lymphocyte degranulation in syntaxin-11 deficient familial hemophagocytic lymphohistiocytosis 4 (FHL4) patients. Blood 2007;110:1906–1915. [PubMed: 17525286]
15. Jacobelli J, Chmura SA, Buxton DB, Davis MM, Krummel MF. A single class II myosin modulates T cell motility and stopping, but not synapse formation. Nat Immunol 2004;5:531–538. [PubMed: 15064761]
16. Andzelm MM, Chen X, Krzewski K, Orange JS, Strominger JL. Myosin IIA is required for cytolytic granule exocytosis in human NK cells. J Exp Med 2007;204:2285–2291. [PubMed: 17875677]
17. Ludowyke RI, Elgundi Z, Kranenburg T, Stehn JR, Schmitz-Peiffer C, Hughes WE, Biden TJ. Phosphorylation of nonmuscle myosin heavy chain IIA on Ser1917 is mediated by protein kinase C beta II and coincides with the onset of stimulated degranulation of RBL-2H3 mast cells. J Immunol 2006;177:1492–1499. [PubMed: 16849455]
18. Lee S, Rivero F, Park KC, Huang E, Funamoto S, Firtel RA. Dictyostelium PAKc is required for proper chemotaxis. Mol Biol Cell 2004;15:5456–5469. [PubMed: 15483055]
19. Geisbrecht ER, Montell DJ. Myosin VI is required for E-cadherin-mediated border cell migration. Nat Cell Biol 2002;4:616–620. [PubMed: 12134162]

20. Deng W, Leaper K, Bownes M. A targeted gene silencing technique shows that Drosophila myosin VI is required for egg chamber and imaginal disc morphogenesis. J Cell Sci 1999;112(Pt 21):3677–3690. [PubMed: 10523504]
21. Krzewski K, Chen X, Orange JS, Strominger JL. Formation of a WIP-, WASp-, actin-, and myosin IIA-containing multiprotein complex in activated NK cells and its alteration by KIR inhibitory signaling. J Cell Biol 2006;173:121–132. [PubMed: 16606694]
22. Sellers JR. Myosins: a diverse superfamily. Biochim Biophys Acta 2000;1496:3–22. [PubMed: 10722873]
23. Eddinger TJ, Meer DP. Myosin II isoforms in smooth muscle: heterogeneity and function. Am J Physiol Cell Physiol 2007;293:C493–508. [PubMed: 17475667]
24. Ikebe M, Komatsu S, Woodhead JL, Mabuchi K, Ikebe R, Saito J, Craig R, Higashihara M. The tip of the coiled-coil rod determines the filament formation of smooth muscle and nonmuscle myosin. J Biol Chem 2001;276:30293–30300. [PubMed: 11395487]
25. Nyitray L, Mocz G, Szilagyi L, Balint M, Lu RC, Wong A, Gergely J. The proteolytic substructure of light meromyosin. Localization of a region responsible for the low ionic strength insolubility of myosin. J Biol Chem 1983;258:13213–13220. [PubMed: 6355107]
26. Cross RA, Vandekerckhove J. Solubility-determining domain of smooth muscle myosin rod. FEBS Lett 1986;200:355–360. [PubMed: 3709799]
27. Sinard JH, Rimm DL, Pollard TD. Identification of functional regions on the tail of Acanthamoeba myosin-II using recombinant fusion proteins. II. Assembly properties of tails with NH2- and COOH-terminal deletions. J Cell Biol 1990;111:2417–2426. [PubMed: 2177477]
28. Straight AF, Cheung A, Limouze J, Chen I, Westwood NJ, Sellers JR, Mitchison TJ. Dissecting temporal and spatial control of cytokinesis with a myosin II Inhibitor. Science 2003;299:1743–1747. [PubMed: 12637748]
29. Saitoh M, Ishikawa T, Matsushima S, Naka M, Hidaka H. Selective inhibition of catalytic activity of smooth muscle myosin light chain kinase. J Biol Chem 1987;262:7796–7801. [PubMed: 3108259]
30. Seri M, Cusano R, Gangarossa S, Caridi G, Bordo D, Lo Nigro C, Ghiggeri GM, Ravazzolo R, Savino M, Del Vecchio M, d'Apolito M, Iolascon A, Zelante LL, Savoia A, Balduini CL, Noris P, Magrini U, Belletti S, Heath KE, Babcock M, Glucksman MJ, Aliprandis E, Bizzaro N, Desnick RJ, Martignetti JA. Mutations in MYH9 result in the May-Hegglin anomaly, and Fechtner and Sebastian syndromes. The May-Heggllin/Fechtner Syndrome Consortium. Nat Genet 2000;26:103–105. [PubMed: 10973259]
31. Seri M, Pecci A, Di Bari F, Cusano R, Savino M, Panza E, Nigro A, Noris P, Gangarossa S, Rocca B, Gresele P, Bizzaro N, Malatesta P, Koivisto PA, Longo I, Musso R, Pecoraro C, Iolascon A, Magrini U, Rodriguez Soriano J, Renieri A, Ghiggeri GM, Ravazzolo R, Balduini CL, Savoia A. MYH9-related disease: May-Hegglin anomaly, Sebastian syndrome, Fechtner syndrome, and Epstein syndrome are not distinct entities but represent a variable expression of a single illness. Medicine (Baltimore) 2003;82:203–215. [PubMed: 12792306]
32. Kelley MJ, Jawien W, Ortel TL, Korczak JF. Mutation of MYH9, encoding non-muscle myosin heavy chain A, in May-Hegglin anomaly. Nat Genet 2000;26:106–108. [PubMed: 10973260]
33. Heath KE, Campos-Barros A, Toren A, Rozenfeld-Granot G, Carlsson LE, Savige J, Denison JC, Gregory MC, White JG, Barker DF, Greinacher A, Epstein CJ, Glucksman MJ, Martignetti JA. Nonmuscle myosin heavy chain IIA mutations define a spectrum of autosomal dominant macrothrombocytopenias: May-Hegglin anomaly and Fechtner, Sebastian, Epstein, and Alport-like syndromes. Am J Hum Genet 2001;69:1033–1045. [PubMed: 11590545]
34. Orange JS, Ramesh N, Remold-O'Donnell E, Sasahara Y, Koopman L, Byrne M, Bonilla FA, Rosen FS, Geha RS, Strominger JL. Wiskott-Aldrich syndrome protein is required for NK cell cytotoxicity and colocalizes with actin to NK cell-activating immunologic synapses. Proc Natl Acad Sci U S A 2002;99:11351–11356. [PubMed: 12177428]
35. Vahlne G, Becker S, Brodin P, Johansson MH. IFN-gamma production and degranulation are differentially regulated in response to stimulation in murine natural killer cells. Scand J Immunol 2008;67:1–11. [PubMed: 18028287]
36. Yanagida T, Arata T, Oosawa F. Sliding distance of actin filament induced by a myosin crossbridge during one ATP hydrolysis cycle. Nature 1985;316:366–369. [PubMed: 4022127]

37. Kolega J. Phototoxicity and photoinactivation of blebbistatin in UV and visible light. Biochem Biophys Res Commun 2004;320:1020–1025. [PubMed: 15240150]
38. Burkhardt JK, Hester S, Lapham CK, Argon Y. The lytic granules of natural killer cells are dual-function organelles combining secretory and pre-lysosomal compartments. J Cell Biol 1990;111:2327–2340. [PubMed: 2277062]
39. Stinchcombe JC, Bossi G, Booth S, Griffiths GM. The immunological synapse of CTL contains a secretory domain and membrane bridges. Immunity 2001;15:751–761. [PubMed: 11728337]
40. Vyas YM, Mehta KM, Morgan M, Maniar H, Butros L, Jung S, Burkhardt JK, Dupont B. Spatial organization of signal transduction molecules in the NK cell immune synapses during MHC class I-regulated noncytolytic and cytolytic interactions. J Immunol 2001;167:4358–4367. [PubMed: 11591760]
41. Langford GM. Myosin-V, a versatile motor for short-range vesicle transport. Traffic 2002;3:859–865. [PubMed: 12453149]
42. DePina AS, Langford GM. Vesicle transport: the role of actin filaments and myosin motors. Microsc Res Tech 1999;47:93–106. [PubMed: 10523788]
43. Heimann K, Percival JM, Weinberger R, Gunning P, Stow JL. Specific isoforms of actin-binding proteins on distinct populations of Golgi-derived vesicles. J Biol Chem 1999;274:10743–10750. [PubMed: 10196146]
44. Ikonen E, de Almeid JB, Fath KR, Burgess DR, Ashman K, Simons K, Stow JL. Myosin II is associated with Golgi membranes: identification of p200 as nonmuscle myosin II on Golgi-derived vesicles. J Cell Sci 1997;110(Pt 18):2155–2164. [PubMed: 9378765]
45. DePina AS, Wollert T, Langford GM. Membrane associated nonmuscle myosin II functions as a motor for actin-based vesicle transport in clam oocyte extracts. Cell Motil Cytoskeleton 2007;64:739–755. [PubMed: 17630664]
46. Neco P, Fernandez-Peruchena C, Navas S, Gutierrez LM, de Toledo GA, Ales E. Myosin II contributes to fusion pore expansion during exocytosis. J Biol Chem 2008;283:10949–10957. [PubMed: 18283106]
47. Neco P, Giner D, Viniegra S, Borges R, Villarroel A, Gutierrez LM. New roles of myosin II during vesicle transport and fusion in chromaffin cells. J Biol Chem 2004;279:27450–27457. [PubMed: 15069078]
48. Holst J, Sim AT, Ludowyke RI. Protein phosphatases 1 and 2A transiently associate with myosin during the peak rate of secretion from mast cells. Mol Biol Cell 2002;13:1083–1098. [PubMed: 11907284]
49. Murakami N, Elzinga M, Singh SS, Chauhan VP. Direct binding of myosin II to phospholipid vesicles via tail regions and phosphorylation of the heavy chains by protein kinase C. J Biol Chem 1994;269:16082–16090. [PubMed: 8206908]
50. Li D, Miller M, Chantler PD. Association of a cellular myosin II with anionic phospholipids and the neuronal plasma membrane. Proc Natl Acad Sci U S A 1994;91:853–857. [PubMed: 8302857]
51. Wu X, Sakamoto T, Zhang F, Sellers JR, Hammer JA 3rd. In vitro reconstitution of a transport complex containing Rab27a, melanophilin and myosin Va. FEBS Lett 2006;580:5863–5868. [PubMed: 17045265]
52. Krzewski K, Chen X, Strominger JL. WIP is essential for lytic granule polarization and NK cell cytotoxicity. Proc Natl Acad Sci U S A 2008;105:2568–2573. [PubMed: 18258743]
53. Casey TM, Meade JL, Hewitt EW. Organelle proteomics: identification of the exocytic machinery associated with the natural killer cell secretory lysosome. Mol Cell Proteomics 2007;6:767–780. [PubMed: 17272266]
54. Colucci F, Rosmaraki E, Bregenholt S, Samson SI, Di Bartolo V, Turner M, Vanes L, Tybulewicz V, Di Santo JP. Functional dichotomy in natural killer cell signaling: Vav1-dependent and -independent mechanisms. J Exp Med 2001;193:1413–1424. [PubMed: 11413196]
55. Berg RE, Crossley E, Murray S, Forman J. Relative contributions of NK and CD8 T cells to IFN-gamma mediated innate immune protection against Listeria monocytogenes. J Immunol 2005;175:1751–1757. [PubMed: 16034116]

56. Franke JD, Dong F, Rickoll WL, Kelley MJ, Kiehart DP. Rod mutations associated with MYH9-related disorders disrupt nonmuscle myosin-IIA assembly. Blood 2005;105:161–169. [PubMed: 15339844]

57. De La Cruz EM, Ostap EM. Relating biochemistry and function in the myosin superfamily. Curr Opin Cell Biol 2004;16:61–67. [PubMed: 15037306]

58. Murakami N V, Chauhan P, Elzinga M. Two nonmuscle myosin II heavy chain isoforms expressed in rabbit brains: filament forming properties, the effects of phosphorylation by protein kinase C and casein kinase II, and location of the phosphorylation sites. Biochemistry 1998;37:1989–2003. [PubMed: 9485326]

59. Conti MA, Sellers JR, Adelstein RS, Elzinga M. Identification of the serine residue phosphorylated by protein kinase C in vertebrate nonmuscle myosin heavy chains. Biochemistry 1991;30:966–970. [PubMed: 1899200]

60. Moussavi RS, Kelley CA, Adelstein RS. Phosphorylation of vertebrate nonmuscle and smooth muscle myosin heavy chains and light chains. Mol Cell Biochem 1993;127–128:219–227.

61. Kriajevska M, Tarabykina S, Bronstein I, Maitland N, Lomonosov M, Hansen K, Georgiev G, Lukanidin E. Metastasis-associated Mts1 (S100A4) protein modulates protein kinase C phosphorylation of the heavy chain of nonmuscle myosin. J Biol Chem 1998;273:9852–9856. [PubMed: 9545325]

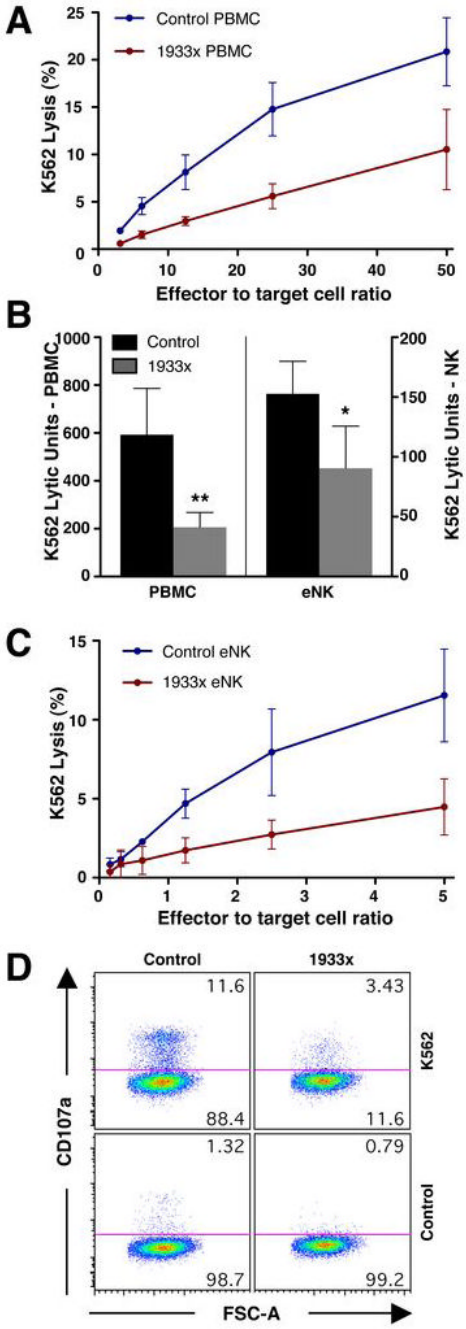

Figure 1.

Effect of myosin IIA 1933x mutation on cytotoxicity and perforin localization at the IS. **(A)** Cytotoxicity of control donor (blue) and myosin IIA 1933x patient (red) PBMCs against K562 target cells. Mean ±SD specific K562 ^{51}Cr-release from 3 separate control donors and patients is shown. Individual experiments were performed in triplicate and averages of these were used to calculate means of the patients or controls ± SD. **(B)** Mean K562 lytic units ±SD of PBMCs and eNK cells from 4 control donors (black) and myosin IIA 1933x patients (gray). Patient and control means were compared using the exact Wilcoxon-Mann-Whitney test: **p=0.014 for PBMCs and *p=0.05 for eNK cells. **(C)** Cytotoxicity of control donor (blue) and myosin IIA 1933x patient (red) eNK cells against K562 target cells. Mean ±SD specific ^{51}Cr-release from

3 separate control donors and patients is shown. **(D)** Flow cytometric analysis depicting CD107a exposure in $CD3^{-}CD4^{-}CD56^{+}$ cells from control donor and myosin IIA 1933x patient PBMC populations mixed with DMSO or K562 cells.

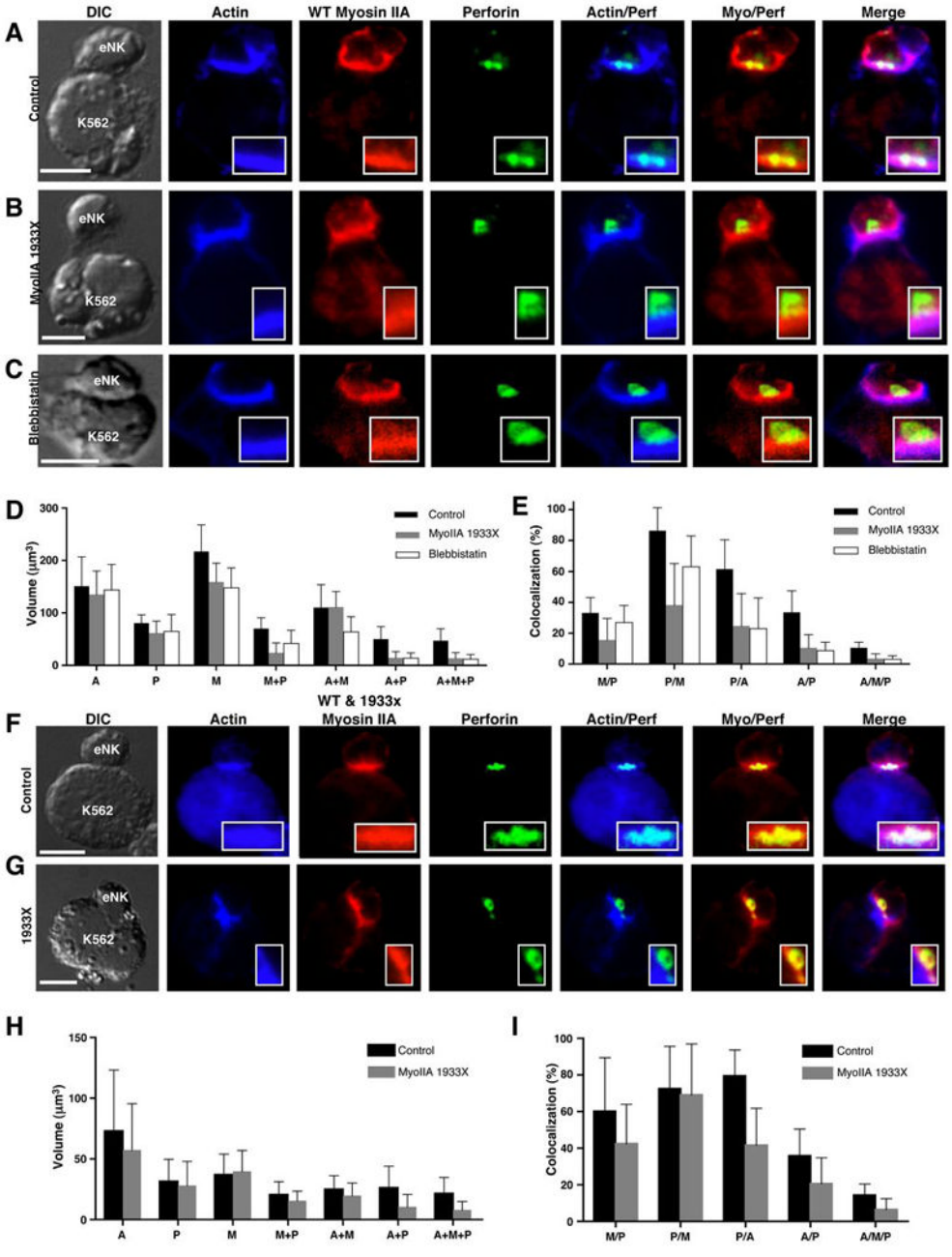

Figure 2.

Confocal fluorescent micrographs of control donor **(A,F)**, myosin IIA 1933X patient 1 and 3 **(B,G)**, and blebbistatin-treated control **(C)** eNK cells conjugated with K562 target cells. Differential interference contrast (DIC), actin (blue), wild-type myosin IIA (red), perforin (green), and overlays are shown. Scale bar = 5 μm. Anti-myosin IIA antibodies were utilized that recognize wild-type **(A–C)** or both mutant and wild-type forms **(F–G). (D,H)** Mean volume ±SD occupied by actin (A), perforin (P), myosin IIA (M), or a combination is shown for control (black), myosin IIA 1933X patient (gray), and blebbistatin-treated (white, D only) eNK cells conjugated with K562 cells. **(E, I)** Mean percent colocalization ±SD among the fluorescent volumes in control (black), myosin IIA 1933X patient (gray), and blebbistatin-treated (white, E only) eNK cells conjugated with K562 cells. The percentage of myosin IIA

colocalized with perforin (M/P), perforin with myosin (P/M), perforin with actin (P/A), actin with perforin (A/P), and actin with myosin and perforin (A/M/P) are shown. ≥10 cells per condition are represented.

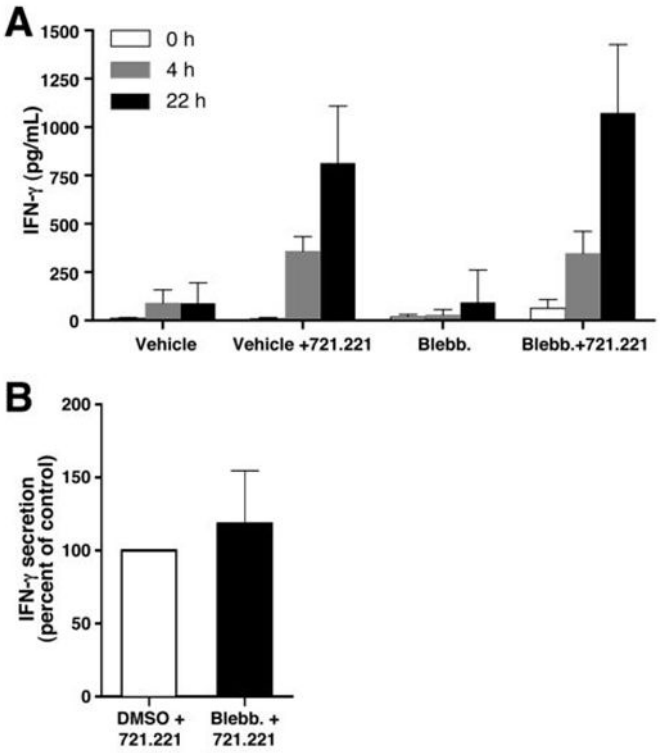

Figure 3.

Effect of inhibition of myosin IIA on NK cell IFN-γ secretion. **(A)** YTS cells incubated with DMSO vehicle control or blebbistatin for 30 min and then incubated in the presence or absence of 721.221 target cells at a 2:1 effector to target cell ratio for 0h (white), 4h (gray), or 22h (black). IFN-γ secreted into supernatant was measured by ELISA. Values shown are the mean ±SD of six independent experiments, each performed on a separate date. **(B)** IFN-γ secretion by vehicle- or blebbistatin-treated control donor eNK cells incubated in the presence of 721.221 target cells at a 2:1 effector to target ratio for 22h. In each experiment, the IFN-γ secreted by blebbistatin-treated eNK cells was normalized to the control (which is shown as 100%) and the values shown are the mean ±SD of three independent experiments, each performed on a separate date.

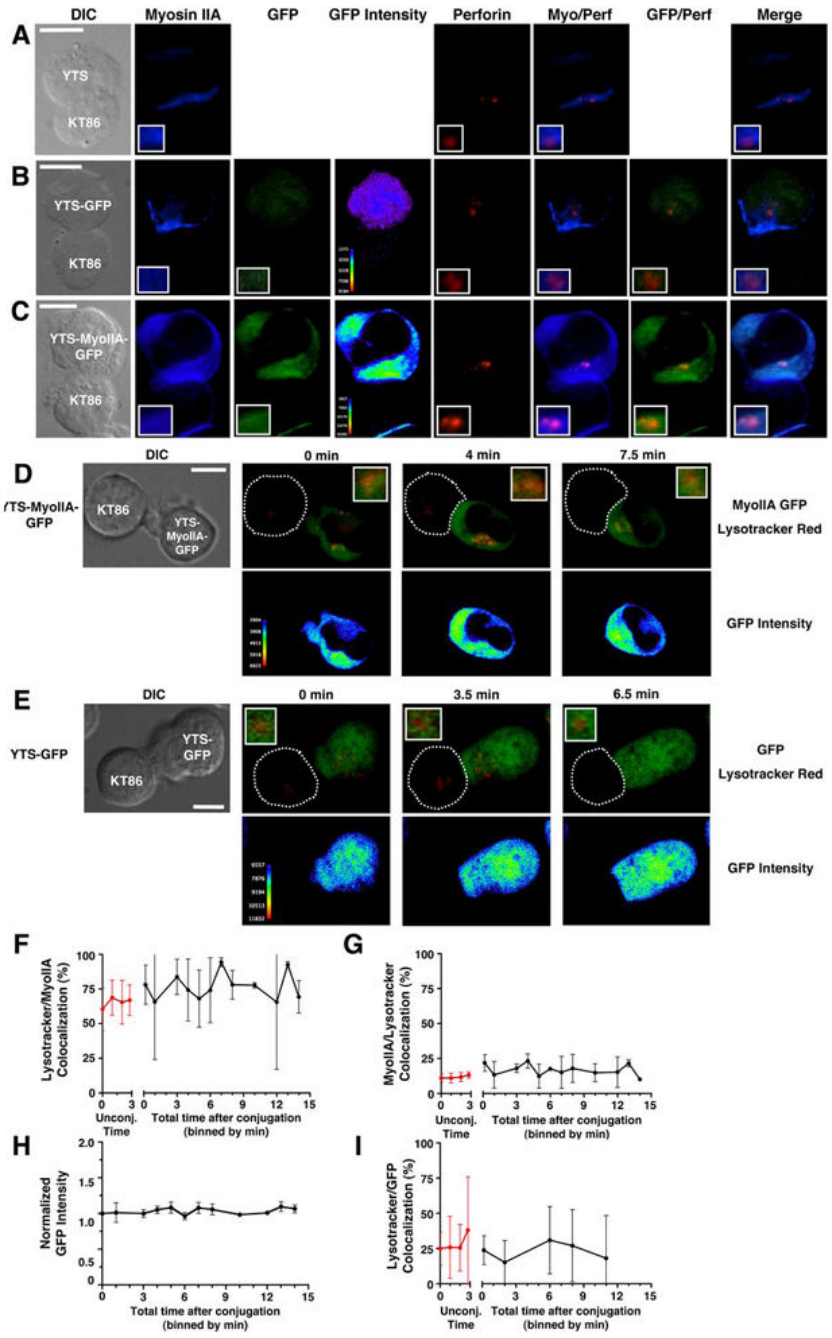

Figure 4.

Myosin IIA colocalization with lytic granules in fixed **(A–C)** and live **(D–I)** NK cells. **(A–C)** Cytolytic conjugates between YTS **(A)** YTS-GFP **(B)**, or YTS-Myosin IIA-GFP **(C)** cells and a KT86 target cell. Differential interference contrast (DIC) and confocal fluorescent images for myosin IIA (blue), GFP (green), GFP intensity (rainbow), perforin (red), and overlays of fluorescence are shown. Inset panels in lower left corner show an enlargement of the area containing lytic granules. **(D–E)** Live cell confocal images of Lysotracker Red-loaded YTS-MyoIIA-GFP **(D)** or YTS-GFP **(E)** cells conjugated with KT86 target cells. The DIC image taken at 0 min is shown (left). Top panels show an overlay of Myosin IIA-GFP (YTS-MyoIIA-GFP) or GFP (YTS-GFP) (green) with Lysotracker Red (red); bottom panels use a pseudocolor

scale to show intensity of GFP only (Lysotracker Red fluorescence was removed prior to applying color scale). In all images, an intensity threshold has been applied to the fluorescent signal so that only 3 SD above the mean intensity for each fluorophore is shown. Scale bars = 10 μm. (**F–G)** Mean percent ±SD Lysotracker Red fluorescent area colocalized with myosin IIA-GFP fluorescent area **(F)** and mean percent ±SD myosin IIA-GFP colocalized with Lysotracker Red **(G)** in YTS-Myosin IIA-GFP cells over time after conjugation with KT86 target cells (black lines). Red lines indicate percent colocalized fluorescent areas ±SD in unconjugated cells over time. **(H)** Mean GFP fluorescence intensity ±SD over time at the colocalized area between myosin IIA-GFP and Lysotracker Red after conjugation to target cells. **(I)** Mean percent ±SD Lysotracker Red fluorescent area colocalized with GFP fluorescent area of YTS-GFP cells over time after conjugation with KT86 target cells (black line). Red line indicates percent colocalized area ±SD in unconjugated cells. All graphs represent live cell image sequences of ≥8 conjugates.

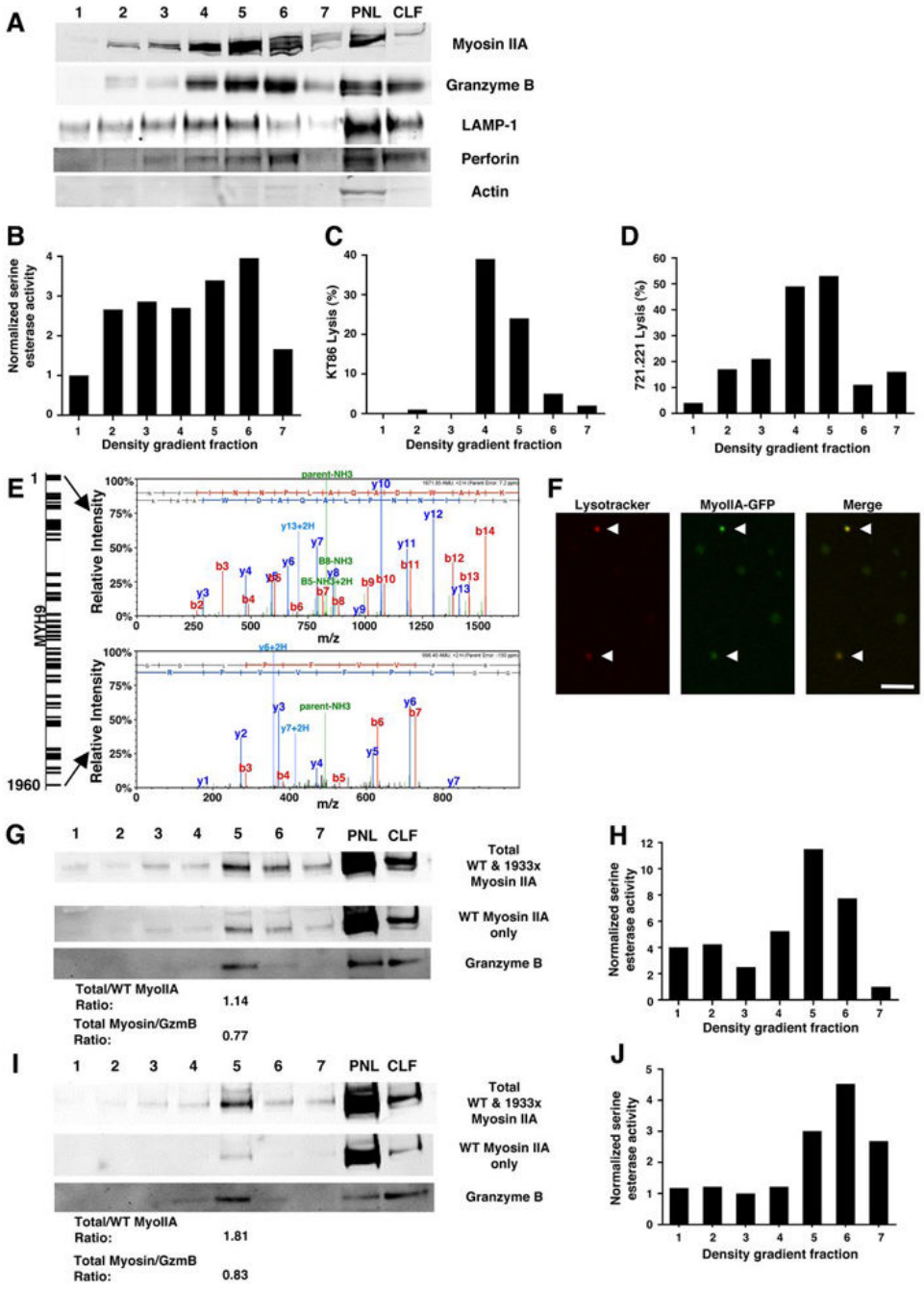

Figure 5.

Evaluation of myosin IIA in isolated NK cell lytic granules. Fractions from density gradient separation of lytic granules from YTS **(A–E)**, YTS-Myosin IIA-GFP **(F)**, control NK **(G–H)**, and 1933X NK **(I–J)** cells. **(A, G, I)** Myosin IIA, granzyme B, LAMP-1, perforin, and actin Western blot of density gradient fractions, from least (1) to most dense (7) as well as the post-nuclear lysate (PNL) and crude lysosomal fraction (CLF) generated in preparing the starting material for the density gradient. In **(G, I)**, anti-myosin IIA antibodies with specificities for both wild type and 1933x myosin IIA (top), or only wild-type myosin IIA (middle). Densitometric ratios of total to wild-type epitope recognizing antibody signal, as well as total myosin IIA to granzyme B, are shown below the Western blots. **(B, H, J)** Serine esterase

activity of YTS **(B)**, control NK **(H)**, and 1933x NK cell **(J)** density gradient fractions. **(C–D)** Cytotoxicity of KT86 **(C)** and 721.221 **(D)** target cells mediated by YTS density gradient fractions. **(E)** Mass spectrometric analysis of peptides identified in a density gradient fraction from YTS cells enriched in myosin IIA and granzyme B, identifying MYH9 in the bands demonstrated in the Western blots. The diagram (left) depicts peptide coverage of MYH9, and the mass spectra (right) represent the most N-terminal and most C-terminal peptides identified. **(F)** Confocal fluorescent images of isolated lytic granules from YTS-Myosin IIA-GFP cells (gradient fractions 5 and 6) loaded with Lysotracker Red. Presumed lytic granules (arrows) demonstrated both Lysotracker (red) and myosin IIA-GFP (green) fluorescence. Scale bar = 4 μm.

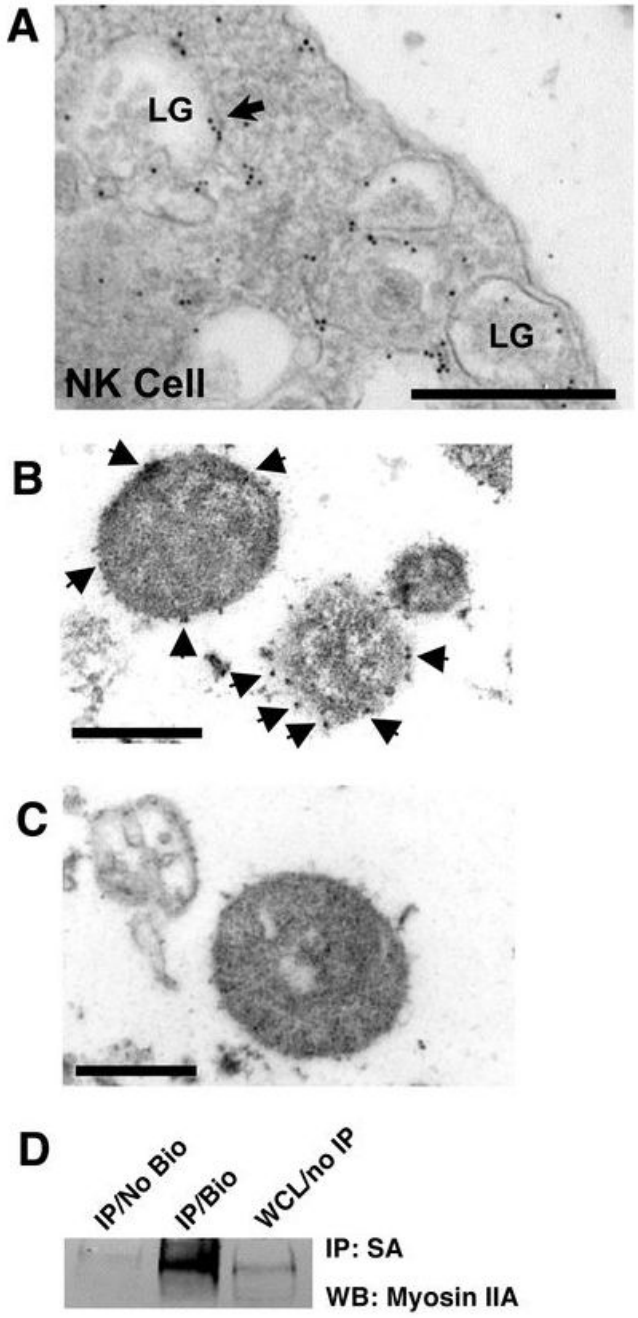

Figure 6.

Ultrastructural localization of myosin IIA in NK cells and isolated lytic granules. **(A)** Electron micrograph of an unconjugated eNK cell stained with rabbit anti-myosin IIA Ab followed by gold-conjugated anti-rabbit Ab. LG = lytic granule. Arrows indicate areas containing gold particles. Scale bar = 500 nm. **(B)** Electron micrograph of isolated lytic granules from YTS cells stained with rabbit anti-myosin IIA Ab followed by gold-conjugated anti-rabbit Ab. Arrows indicate areas containing gold particles. Scale bar = 500 nm. **(C)** Electron micrograph of isolated lytic granules from YTS cells stained with gold-conjugated anti-rabbit Ab alone. Scale bar = 500 nm. Arrows indicate gold particles. **(D)** Western blot of streptavidin-agarose

immunoprecipitates from unlabeled lytic granules (No Bio) and surface-biotinylated lytic granules (Bio), and whole cell lysate (WCL) from YTS cells.

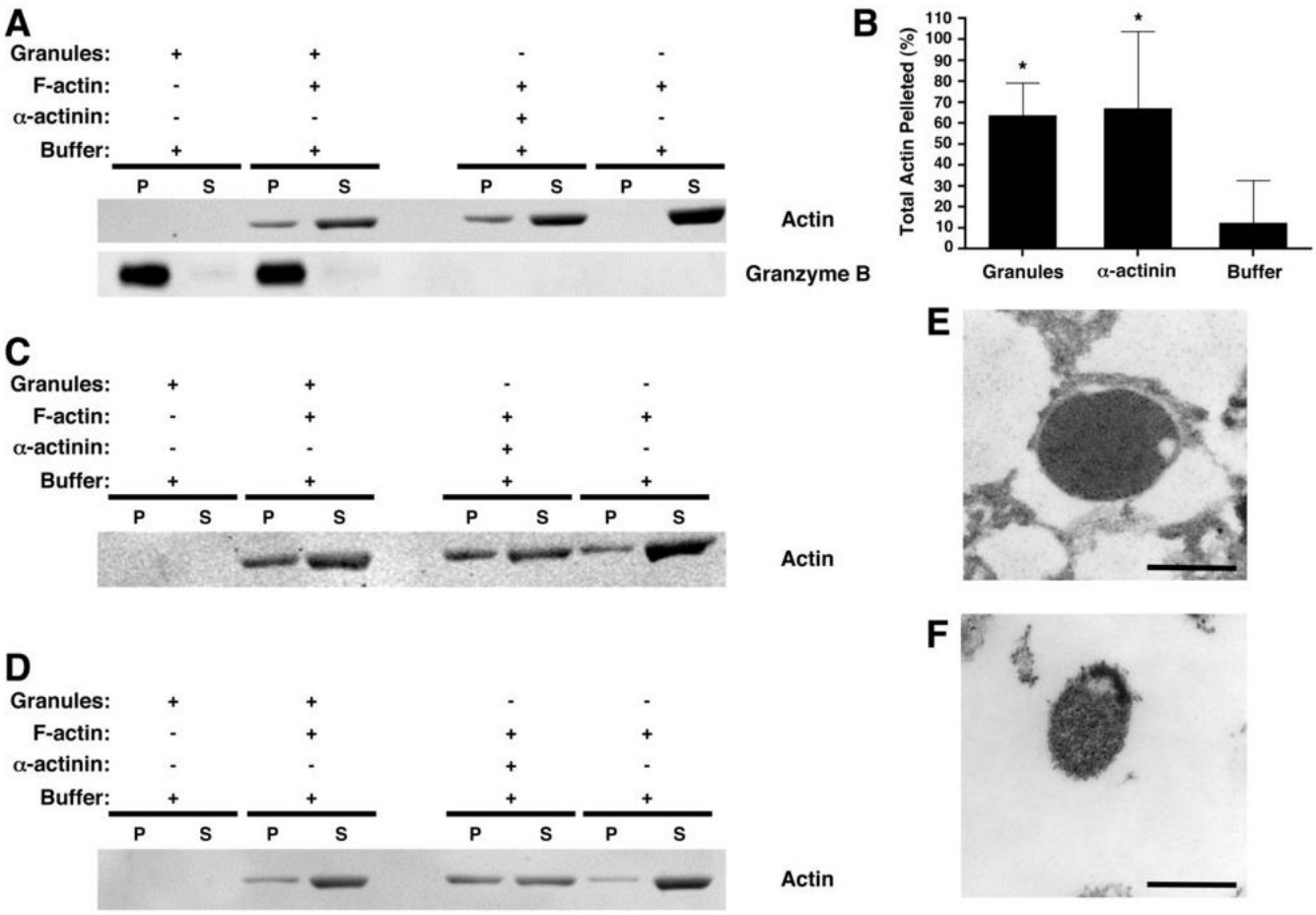

Figure 7.

Interaction between myosin IIA-associated lytic granules and F-actin. Lytic granules from an isolated fraction enriched in myosin IIA and granzyme B were prepared from YTS **(A–B, E–F)**, control NK **(C)**, and myosin IIA 1933x patient NK **(D)** and incubated for 30 min in the presence or absence of F-actin. After centrifugation at 18,000*g*, the pellet (P) and supernatant (S) were evaluated for actin and granzyme B by Western blot **(A, C, D)**. As a positive control, α-actinin was used to bundle the F-actin, causing it to pellet. Pellet and supernatant from the assay were separated. **(B)** Percentage of actin in the pellet ±SD from three independent experiments, determined by densitometric analysis. *= $p<0.05$ compared to buffer (negative control). **(E–F)** Electron micrographs of lytic granule pellets. The pellet obtained from the mixture of lytic granules and F-actin **(E)** was compared to the pellet of lytic granules alone **(F)**. Scale bar = 500 nm.

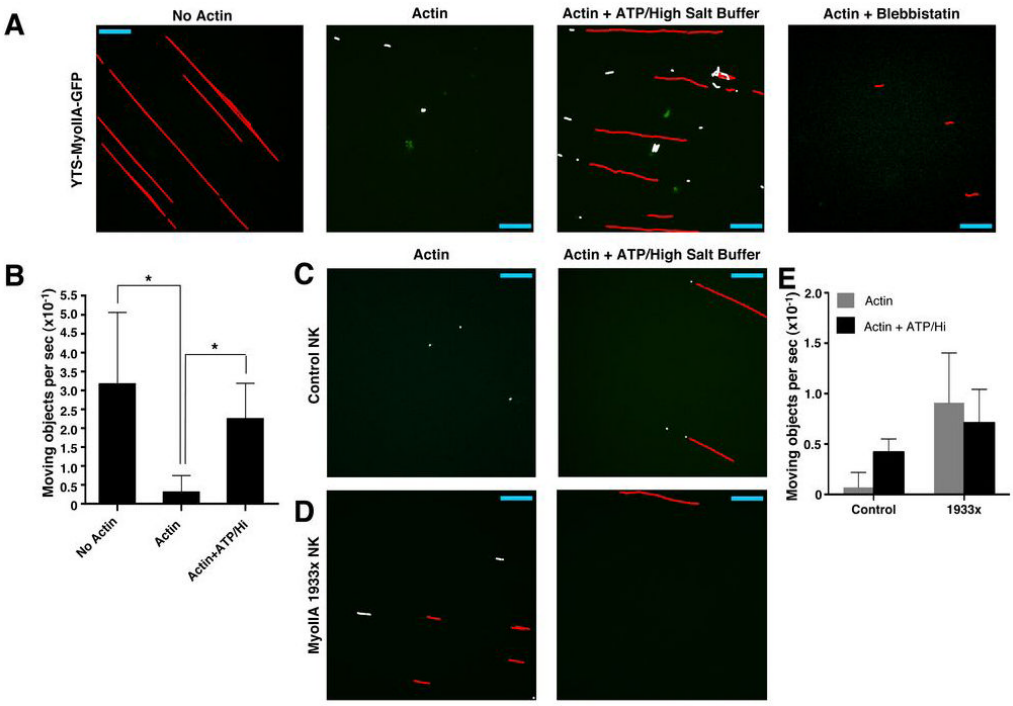

Figure 8.

Functional association of lytic granules with F-actin and effects of ATP and myosin IIA 1933x. Isolated lytic granules were added to flow chambers containing biotinylated BSA/streptavidin (BSA/SA) without actin, with actin and physiologic salt buffer, or with actin and ATP-containing high-salt buffer, or with actin using blebbistatin-treated granules. Granules from YTS-MyoIIA-GFP **(A)**, control NK **(C)**, and 1933x NK **(D)** cells were drawn through the chamber and allowed to flow through or adhere for 1–2 min before imaging with a confocal microscope at approx. 5 time points per second. From any single culture propagated NK cell preparation the quantity of lytic granules obtained was sufficient for flow through only two chambers. Images were analyzed using the object tracking function in Volocity software and represent an overlay of 12 to 45 seconds. Individual moving objects which had displacement greater than 5 μm (red) and displacement less than 5 μm (white) are indicated. Scale bar = 40 μm. Some images are rotated from their original orientation, shown in **Supplementary Videos 4A–6B. (B)** Number of moving objects per second ±SD in 3–5 independent sequences of isolated YTS-Myosin IIA-GFP lytic granules added to flow chambers. *= $p<0.05$.

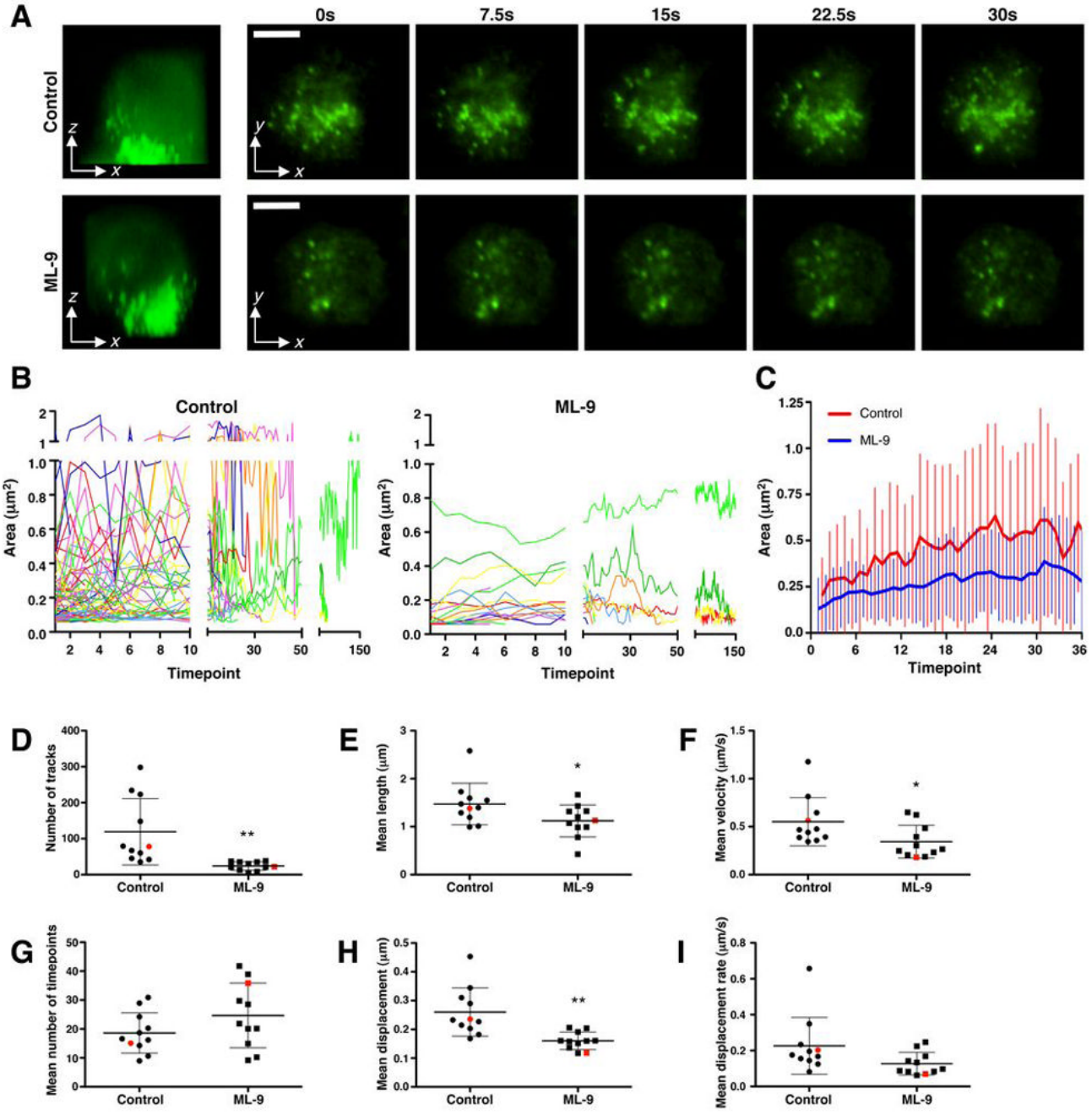

Figure 9.

Evaluation of myosin IIA in lytic granule dynamics. **(A)** Control or ML-9-treated YTS cells with polarized lytic granules (as determined by confocal fluorescent microscopy, at left) were imaged on an anti-CD28-coated glass surface using TIRFm for 30 seconds at a rate of 5 images per second. Scale bar = 5 μm. Representative cells of 11 individually analyzed cells for each condition are shown and were chosen based upon their representation of the median number of tracks of all cells analyzed. **(B)** Change in area over time for individual granules in the representative cells. *y-axis* was divided at 1 μm^2 as exceeding values were likely not to represent individual granules but rather conglomerates. (**C**) Mean ±SD lytic granule area for the cells depicted in **(A,B)** is shown over the number of timepoints representing the mean duration of

tracks in ML-9-treated cells. The mean number of timepoints in the control-treated YTS cell tracks (red) was less than in the ML-9-treated cells (blue). **(D–I)** The total number of tracks **(D)**, mean track length **(E)**, mean track velocity **(F)**, mean number of timepoints for tracks **(G)**, mean track displacement **(H)**, mean track displacement rate **(I)** plotted to show each of 11 independent control and ML-9-treated replicate cells, ±SD. Red points in each condition indicate the representative cell shown in **(A)** and **(B)**. Difference between the means of control and ML-9-treated cells in **(D,E,F,H)** was significant ($p<0.05$), and in **(I)** demonstrates a trend ($p<0.1$).